








An $\alpha 7$ nicotinic and GABA_B receptor-mediated pathway controls acetylcholine release in the tripartite neuromuscular junction

Konstantin Petrov^{1,2}, Oksana Lenina¹ , Jacqueline Leroy³, Véronique Bernard⁴ , Thibaut Germain⁵ , Charles Truong⁵ , Leniz Nurullin^{2,6}, Guzel Sibgatullina² , Kinji Ohno⁷ , Dmitry Samigullin^{2,8} and Eric Krejci³ 

¹Arbuzov Institute of Organic and Physical Chemistry, FRC Kazan Scientific Center of RAS, Kazan, Russia

²Kazan Institute of Biochemistry and Biophysics, FRC Kazan Scientific Center of RAS, Kazan, Russia

³Université Paris Cité, CNRS, ENS Paris Saclay, Centre Borelli UMR 9010, Paris, France

⁴Sorbonne Université, CNRS UMR 8246-INSERM U1130, Paris, France

⁵Université Paris Saclay, CNRS, ENS Paris Saclay, Centre Borelli UMR 9010, Gif sur Yvette, France

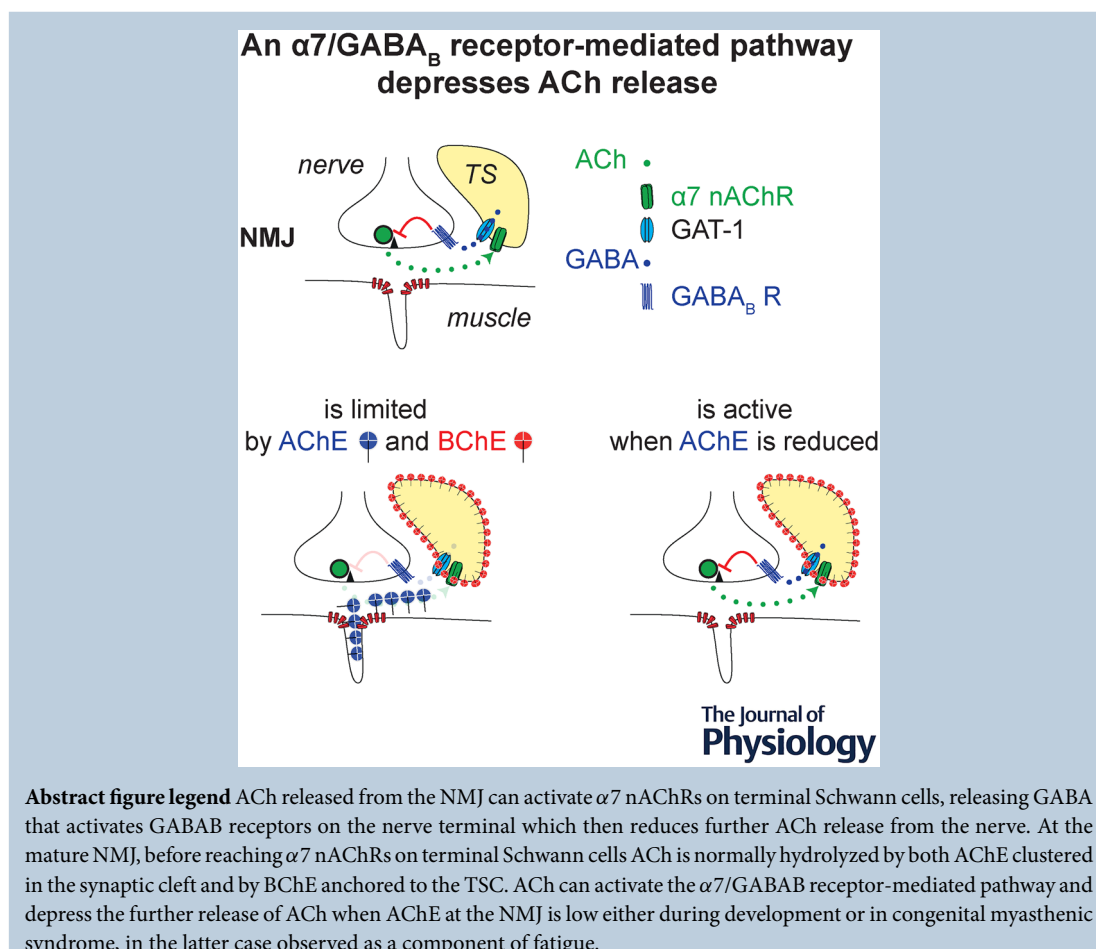
⁶Kazan State Medical University, Kazan, Russia

⁷Graduate School of Nutritional Sciences, Nagoya University of Arts and Sciences, Nisshin, Japan

⁸Department of Radiophotonics and Microwave Technologies, Kazan National Research Technical University Named after A.N. Tupolev-KAI, Kazan, Russia

Handling Editors: Katalin Toth & Samuel Young

The peer review history is available in the Supporting Information section of this article (<https://doi.org/10.1113/JP287243#support-information-section>).



Abstract Terminal Schwann cells (TSCs) are capable of regulating acetylcholine (ACh) release at the neuromuscular junction (NMJ). We have identified GABA as a gliotransmitter at mouse NMJs. When ACh activates $\alpha 7$ nicotinic ACh receptor (nAChRs) on TSCs, GABA is released and activates GABA_B receptors on the nerve terminal that subsequently reduce ACh release. Indeed, specific deletion of the $\alpha 7$ nAChR in TSCs or inhibition of the metabotropic GABA_B receptor prevents the reduction in the quantal content of the end-plate potential induced by cholinesterase inhibitors. The $\alpha 7$ /GABA_B receptor-mediated pathway is activated when ACh that escapes from collagen Q (ColQ) anchored AChE in the synaptic cleft and from PRiMA-anchored butyrylcholinesterase on the TSC activates $\alpha 7$ nAChRs on the TSC. Consequently, prolonged tetanic stimulation of isolated muscle activates the $\alpha 7$ /GABA_B receptor pathway, which reduces post-tetanic ACh release. When AChE levels are low in neonatal mice, the $\alpha 7$ /GABA_B receptor-mediated pathway decreases ACh release and reduces *ex vivo* muscle fatigue. For ColQ-deficient mice where AChE is not clustered, the decrease in ACh release following activation of this pathway contributes to mouse fatigue *in vivo*.

(Received 6 July 2024; accepted after revision 13 November 2024; first published online 30 December 2024)

Corresponding author E. Krejci: Université Paris Cité, CNRS, ENS Paris Saclay, Centre Borelli UMR 9010, Paris, France.
Email: eric.krejci@parisdescartes.fr

Key points

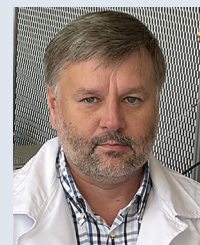
- Acetylcholine (ACh) released from the nerve terminal at the neuromuscular junction (NMJ) can activate $\alpha 7$ nicotinic ACh receptor (nAChR) on terminal Schwann cells, releasing gamma-aminobutyric acid (GABA) that activates metabotropic GABA_B receptors on the nerve terminal which then reduces further ACh release from the nerve.
- At the mature NMJ, before reaching $\alpha 7$ nAChRs on terminal Schwann cells ACh is normally hydrolyzed by AChE clustered in the synaptic cleft and by BChE anchored to the TSC.
- ACh can activate the $\alpha 7$ /GABA_B receptor-mediated pathway and depress subsequent ACh release when AChE at the NMJ is low, either during development or in congenital myasthenic syndrome. In the latter case, this pathway contributes to muscle fatigue.

Introduction

The neuromuscular junction (NMJ) is the synapse responsible for the chemical transmission of electrical impulses from motor neurons to muscle cells. In vertebrates, acetylcholine (ACh) released from the motor nerve terminal acts on the nearby surface of the target muscle fibre where ACh nicotinic receptors (nAChRs) of the muscle type $[(\alpha 1)2\beta 1\gamma \epsilon]$ are localized (Slater, 2017). Synchronized activation of clustered muscle nAChRs causes a local post-synaptic depolarization that initiates

an action potential in the muscle fibre. ACh in the synaptic cleft is hydrolysed by acetylcholinesterase (AChE), which is clustered by specific collagen Q (ColQ) in the basal lamina (Bernard et al., 2011; Blotnick-Rubin & Anglister, 2018). AChE both prevents the rebinding of ACh to muscle-type nAChR and limits the ACh spillover. In addition to AChE, butyrylcholinesterase (BChE) is present at the NMJ. BChE is not able to control the activation of muscle nAChRs (Minic et al., 2003) and, indeed, BChE is not detected in the synaptic cleft. However, BChE is abundant on the surface of terminal Schwann cells (TSCs)

Konstantin Petrov obtained his PhD in physiology and pharmacology at Kazan State Medical University in 2006. In 2010–2013, he worked as a postdoc at the Paris Descartes University in Eric Krejci's research team, investigating physiological function of butyrylcholinesterase at the neuromuscular junction. He is now Head of the Centre for Neurochemistry and Pharmacology at the Arbusov Institute of Organic and Physical Chemistry. His main research interests are cholinergic synaptic transmission, medications for the treatment of Alzheimer's disease and protection against poisoning with cholinesterase inhibitors.



(Petrov et al., 2014) where it may limit the activation of $\alpha 7$ nAChR.

TSCs are specialized glial cells that cover motor nerve terminals and assist in many of their functions (Fuertes-Alvarez & Izeta, 2021). In particular, TSCs can modulate ACh release from the nerve using ATP or adenosine, resulting in enhanced or inhibited ACh release, depending on the nerve discharge pattern (Ko & Robitaille, 2015). Long trains of high frequency nerve stimulation induce Ca^{2+} waves in TSCs, provoking the release of ATP from these cells as a gliotransmitter. ATP secreted from TSCs can be cleaved extracellularly to adenosine, which can inhibit or facilitate ACh release via activation of A1 or A2 adenosine receptors, respectively (Todd et al., 2010). Alternatively, adenosine itself can be secreted during Ca^{2+} waves in TSCs via ENT1 transporters (Noronha-Matos et al., 2020).

We have previously shown that inhibition of BChE at the NMJ depresses ACh release via activation of $\alpha 7$ nAChRs (Petrov et al., 2014). Because BChE is anchored to the surface of TSCs, we proposed that ACh spillover (ACh not hydrolysed by AChE at the synaptic cleft), activates $\alpha 7$ nAChRs, which are presumably localized at the TSCs. However, under our experimental conditions, it remained unclear whether, activation of $\alpha 7$ nAChRs provokes release of ATP, or adenosine release from TSCs, or whether another gliotransmitter is involved.

The present study aimed to: (1) evaluate novel components of this $\alpha 7$ nAChR signalling and (2) identify physiological and pathological conditions under which $\alpha 7$ nAChR-mediated depression of ACh release may result in functional alteration.

Here, we find that when ACh is not hydrolysed by AChE in the synaptic cleft and is not hydrolysed by BChE on TSCs, activation of $\alpha 7$ nAChR of TSCs causes the secretion of GABA, possibly by reversing the mode of action of the GAT-1 transporter. This GABA release then reduces ACh release by activating metabotropic GABA_B receptors. We then established that (1) the $\alpha 7/\text{GABA}_B$ receptor-mediated pathway induces post-tetanic depression of ACh release after continuous motor nerve stimulation (20 Hz, 120 s); (2) the $\alpha 7/\text{GABA}_B$ receptor-mediated pathway is effective in diaphragm muscles of mice at early stages of postnatal development; and (3) the $\alpha 7/\text{GABA}_B$ receptor-mediated pathway affects neuromuscular synaptic transmission and fatigability of mice in a model of congenital myasthenic syndrome (CMS) with AChE deficit caused by mutation of ColQ gene.

Methods

Ethical approval

All experiments were performed following French guidelines for laboratory animal handling approved

by the Animal Committee of the CNRS in accordance with the European Communities Council Directive 86/609/EC; protocol No. 9 – 2013 and Animal Care and Use Committee of FRC Kazan Scientific Center of RAS. At the Central Animal Facility of the UFR Biomédicale on the Saint Germain site of the Université Paris Cité (license number D750607), the project using animals for scientific purposes has been registered under the number APAFIS #45644-2023081409133437 v9 'Study on mice with partial deficits in acetylcholine hydrolysis'. The protocols of experiments were approved by the Animal Care and Use Committee of FRC Kazan Scientific Center of RAS (protocol No. 2 from 9 June 2022)

Mice were maintained in a mixed genetic background derived from B6D2, obtained from Janvier Labs (Le Genest-Saint-Isle, France), avoiding sibling crosses to maintain genetic diversity. Mice were raised in ventilated MICE cages (Innovive, San Diego, CA, USA) with automatic watering, under 12:12 h light/dark photocycle and an average temperature of 22°C. Bedding was corn cob, and a cardboard dome and paper were provided for nest building. Food and water were provided *ad libitum*. Animals were kept in pathogen free environment (FELASA list; <https://felasa.eu>). All mice were handled with the approval of the Institutional Animal Care and Use Committee of Université Paris Cité and FRC Kazan Scientific Center of RAS. All experiments were performed in accordance with approved guidelines and the policies and regulations for animal experiments of *The Journal of Physiology* (Grundy, 2015).

Mice were killed by cervical dislocation followed by decapitation. In this study, we used both female ($n = 84$) and male ($n = 90$) mice aged 2–6 months, except for the developmental studies.

Electrophysiological recordings

Nerve–muscle preparations of hemidiaphragm muscle or levator auris longus (LAL) were pinned in translucent chambers and perfused at a rate of 2–3 mL min⁻¹ with oxygenated (95% O₂, 5% CO₂) Krebs–Ringer solution containing: 154 mM NaCl, 5 mM KCl, 2 mM CaCl₂, 1 mM MgCl₂, 5.0 mM Hepes buffer and 11 mM glucose (pH 7.4). Evoked end plate potentials (EPPs) and spontaneous miniature EPPs (mEPPs) were recorded in the synaptic zone using a standard intracellular microelectrode technique (3 M KCl, resistance 10–15 M Ω) at 20–22°C. To prevent the generation of action potentials and muscle contractions, μ -conotoxin GIIIB (2 μ M; Peptide Institute, Inc., Osaka, Japan) was used for the recording of EPPs. The motor nerve was stimulated via a suction electrode with supramaximal current pulses of 0.1 ms in duration. Recordings were made continuously from the same end-plate before and during the tested treatment. Quantal content of EPPs was calculated by dividing the mean EPP

amplitudes by the mean mEPP amplitude recorded in the same muscle fibre. Only fibres with a stable resting membrane potential at -60 mV or less were analysed.

Post-tetanic depression or potentiation were studied using a 120 s train of motor nerve stimulation at 20 Hz. In the same mouse LAL muscle fibre, 50 EPPs and 100 mEPPs were recorded, then 120 s tetanic stimulation was applied and, after 10 s, 50 EPPs and 100 mEPPs were recorded.

The changes in the level of ACh release under conditions of AChE inhibition cannot be correctly estimated by dividing the mean amplitude of EPP by the mean amplitude of mEPP because of the non-linear summation of the postsynaptic effect of individual ACh (Hartzell et al., 1975). For this reason, the effect of the neostigmine was assessed by the change in the probability of ACh release. The probability of ACh release (m_o) was estimated in low calcium (0.4 mM) high magnesium (6.5 mM) Krebs–Ringer solution by the method of failures (del Castillo & Katz, 1954) in which $m_o = \ln(N/N_o)$, where N represents the number of stimuli and N_o represents the number of failures (i.e. the number of stimuli not followed by an EPP).

In diaphragm muscle of newborn mice at postnatal day (P)2, the coefficient of variation (CV) of EPP amplitude distributions (del Castillo & Katz, 1954) was estimated in low calcium (0.1 mM) and high magnesium (8.0 mM) Krebs–Ringer solution in which $CV = SD/A$, where SD is the standard deviation of EPP amplitudes and A is the mean amplitude of EPP. The 20 EPPs were recorded in the same muscle fibre in the control and after 20 min of application of GABA_B receptor blocker.

Synaptic responses were recorded using an Axoclamp 900A amplifier and digitized using Digidata 1440A (Molecular Devices, San Jose, CA, USA) with WinWCP software (John Dempster, University of Strathclyde, Glasgow, UK). The results are presented as the mean \pm SD of n separate experiments in different muscles. Data were analysed using Student's t test (two-tailed) and differences between the control and experimental values were considered statistically significant at $P < 0.05$.

Ex vivo muscle twitch tension measurements

Ex vivo twitch tension measurements were performed as previously described (Lenina et al., 2020). Hemi-diaphragm muscles with their associated phrenic nerves were bathed in oxygenated Krebs–Ringer solution at 25°C. A force sensor TRI201AD (AD Instruments, Sydney, NSW, Australia) was used for twitch tension measurements. Contractions were evoked by stimulating the phrenic nerve (10 Hz, 30 s) via a suction electrode by supramaximal current pulses, 0.1 ms in duration. Optimal muscle length and stimulation voltage were determined from micromanipulation of muscle length to produce

peak force. Data were recorded using Power Lab system and LabChart 6 software (AD Instruments).

Data are expressed as the mean \pm SD. Statistical significance was assessed by the Mann–Whitney test at $P < 0.05$.

Immunohistochemistry

Isolated muscles were fixed in 2% paraformaldehyde solution for 5 min and washed three times in PBS every 10 min for a period of 30 min. The muscles were then incubated in 0.5% Triton X-100 solution for 30 min, followed 15 min in a blocking solution (prepared in PBS) consisting of 1% bovine serum albumin, 5% normal goat serum and 0.5% Triton X-100.

$\alpha 7$ nAChRs were detected in muscle fibres of LAL after incubation for 15 h at 4°C with anti- $\alpha 7$ biotinylated polyclonal antibody (Skok et al., 1999), at $1 \mu\text{g mL}^{-1}$ (dilution 1:1000) in PBS supplemented with 1% normal goat serum. GABA was detected after incubation for 15 h at 4°C with rabbit polyclonal antibodies (dilution 1:200; Sigma-Aldrich, St Louis, MO, USA; catalog. no. A2052) and GABA_B receptors were detected after incubation with goat polyclonal antibodies against the GABA_BR2 subunit of the metabotropic GABA_B receptor (dilution 1:200; Santa Cruz Biotechnology, Inc, Santa Cruz, CA, USA; catalog. no. sc-31457). GAT-1 was detected after incubation with rabbit polyclonal antibodies against the extracellular epitope of rat GABA transporter (GAT)-1 (dilution 1:200; Alamone Labs, Jerusalem, Israel; catalog. no. AGT-001.).

After this incubation with primary antibodies, the muscles were rinsed in Triton X-100 three times for 30 min and incubated for 1 h at room temperature with streptavidin, or with secondary donkey, anti-goat, or with anti-rabbit antibodies conjugated to Alexa-488 or Alexa-647 (dilution 1:800; Invitrogen, Waltham, MA, USA) and, after washing, incubated with tetramethylrhodamine- α -bungarotoxin (TMR- α -bungarotoxin; Sigma-Aldrich; catalog. no. T0195-5MG) $20 \mu\text{g mL}^{-1}$ for 30 min in the dark at room temperature, to visualize the muscle nAChR (Anderson & Cohen, 1974). As a final step in all these procedures, the preparations were mounted in a special solution of anti-fading reagent (Sigma-Aldrich) on glass slides for microscopic observation using a LSM 510 Meta laser scanning confocal microscope (Carl Zeiss, Jena, Germany) with oil immersion 63 \times objectives. Endplates were identified by the binding of fluorescent TMR- α -bungarotoxin to nAChR. A laser with a wavelength of 488 nm for Alexa-488, 647 nm for Alexa-647 and 543 nm for TMR- α -bungarotoxin was used for image acquisition, and the images were processed using ImageJ (NIH, Bethesda, MD, USA).

To confirm the expression of SOX10-Cre in the TSCs but not in the muscle fibre or nerve, we used two reporter genes: Tomato, a cytoplasm-soluble red fluorescent protein, or Channel rhodopsin (CHR2-EYFP), a membrane protein fused to yellow fluorescent protein (YFP). To this end, we detected the direct presence of Tomato in the cytoplasm of the TSCs in Sox10-Cre; floxStopfloxtomato mice (JAX stock #007914) (Madisen et al., 2010) or of CHR2-EYFP at the membrane of the TSCs in Sox10-Cre; floxStopfloxCHR2-EYFP mice (JAX stock #024109) (Madisen et al., 2012) at diaphragm NMJ. The postsynaptic membrane of the NMJ was identified by the presence of nAChR detected with α -bungarotoxin coupled to Alexa488 (Invitrogen, Thermo Fisher, Waltham, MA, USA; catalog. no. B13422), and the terminal was identified by the presence of the synaptic vesicle protein A (SV2A) with a mouse anti-SV2A monoclonal antibody (dilution 1:500; Developmental Studies Hybridoma Bank, Iowa City, IA, USA; catalog. no. AB_2315387). SV2A antibody was detected with an anti-mouse antibody conjugated to Abberior Star 635P (Abberior, Göttingen, Germany; catalog. no. ST635P-1001-500UG). Alternatively, the direct presence of CHR2-EYFP at the TSC membrane was detected in Sox10-Cre; floxStpfloxCHR2-EYFP mice. The postsynaptic membrane of the NMJ was identified by the presence of nAChR detected with α -bungarotoxin coupled to Alexa594 (Invitrogen, Thermo Fisher; catalog. no. B13423) and the nerve terminal was identified by the presence of the vesicular ACh transporter (vAChT) with a guinea pig anti-vAChT antibody (dilution 1:5000; Cristofari et al., 2022). vAChT antibody was detected with an anti-guinea pig antibody conjugated to Abberior Star 635P (Abberior; catalog. no. ST635P-1006-500UG). After washing, the muscles were mounted in Prolong gold (Thermo Fisher Scientific, Waltham, MA, USA) and the samples were viewed under a 980 FAST Airyscan II (Carl Zeiss).

Calcium imaging of TSC

Mouse LAL nerve–muscle preparations were incubated in oxygenated Krebs–Ringer solution (see section on ‘Electrophysiological recordings’) containing 20 mM fluo-3 AM (Invitrogen), 0.02% pluronic acid (Invitrogen) and 0.5% dimethyl sulfoxide (Sigma-Aldrich) for 60 min at 20°C temperature. Partial chelation of heavy metal ions was achieved with 20 mM tetrakis(2-pyridylmethyl)ethylenediamine (Invitrogen) to limit the binding of these ions to fluo-3 (Rochon et al., 2001). After this loading procedure, the preparation was washed with Krebs–Ringer solution for 15 min. The muscles were then pinned down in a Sylgard (Dow Inc., Midland, MI, USA) coated imaging chamber. Changes in fluorescence (F) intensity were monitored using a

confocal microscope (TCS SP5; Leica, Wetzlar, Germany) equipped with an argon ion laser. Observations were made with a 20 \times water immersion objective (1.00 NA; Leica). The 488 nm laser line was attenuated to 6% intensity and a long-pass filter with cutoff at 515 nm was used to detect the emitted F . Surface NMJs were localized using the transmitted light channel of the confocal microscope. F intensity was measured over the area of the TSC cell body and the relative changes in F intensity were evaluated as a percentage as: $\Delta F/F = (F - F_0)/F_0 \times 100$. A suction electrode was used to stimulate the distal end of transected motor nerve (20 Hz, 120 s). To prevent muscle contractions evoked by transmitter release, we used μ -conotoxin GIIIB (2 μ M; Peptide Institute, Inc.) or low calcium (0.4 mM) high magnesium (6.5 mM) Krebs–Ringer solution (see section on ‘Electrophysiological recordings’). When calcium waves were elicited in a TSC by a burst of nerve stimulations (20 Hz, 120 s), the preparations were allowed to recover for 30 min with or without methyllycaconitine (MLA, 10 nM) to specifically block $\alpha 7$ nAChR; then, a second burst of nerve stimulations (20 Hz, 120 s) was applied and the F intensity was measured.

Alternatively, changes in Ca^{2+} levels in the TSC were recorded in low calcium (0.4 mM) high magnesium (6.5 mM) Krebs–Ringer solution during low-frequency stimulation (0.5 Hz, 100 stimuli), the preparations were allowed to recover for 30 min with or without cholinesterase inhibitor neostigmine (1 μ M) and then a second series of nerve stimulations (0.5 Hz, 100 stimuli) was applied and the F intensity was measured.

Detection of acetylcholinesterase at the NMJ with fluorescent Fasciculin-2

Unlabelled Fasciculin-2 was purchased from Abcam (Cambridge, UK) and was conjugated to Alexa 647 using a Microscale Protein Labelling Kit (Invitrogen). TMR- α -bungarotoxin was purchased from Sigma-Aldrich. Six hemidiaphragm muscles in each experimental group (P0, P1, P7, P14 and P60) were isolated from mice killed by cervical dislocation followed by immediate exsanguination. Isolated muscles were fixed in 4% paraformaldehyde for 20 min; then rinsed several times with PBS for total of 15 min and incubated with Alexa Fluor 647-conjugated Fasciculin-2 (dilution 1:1000) and TMR- α -bungarotoxin (20 μ g mL⁻¹) for 20 min. Fluorescence intensity of labelled AChE at NMJs was determined using a TCS SP5 confocal laser microscope (Leica). The average fluorescence intensity was calculated in digital confocal image scans and expressed as arbitrary units.) using LasAF software (Leica). At least 50 NMJs were analysed in each muscle. Average fluorescence intensity is expressed as the mean \pm SD. Statistical significance was assessed by the Mann–Whitney test compared to adult (P60) mice at $P < 0.05$.

Genetic deletion of *Chrna7* in Schwann cells

To delete *Chrna7*, we used a floxed allele of *Chrna7* ((B6;DBA(Cg)-*Chrna7*tm1.1Ehs/YakelJ) in which exon4 of the $\alpha 7$ nAChRs gene is flanked by LoxP recognized by the recombinase Cre (JAX stock #026965; The Jackson Laboratory, Bar Harbor, ME, USA) (Hernandez et al., 2014). To recombine the LoxP sites in the TSC but not in the motor neuron or muscle fibres, we used the transgenic mouse (Sox10Cre mice) (JAX stock #025807) that expresses Cre recombinase under the promoter of Sox10. To confirm that Sox10Cre mice recombine LoxP sites in the TSC but not in diaphragm muscle fibres or phrenic nerve, we mated Sox10Cre with Tomato male (JAX stock #007914) (Madisen et al., 2010) or CHR2-EYFP male (JAX stock #024109) (Madisen et al., 2012).

Sox10Cre is known to be expressed in the male germline, deleting the target floxed allele in all cells of the embryo (Crispino et al., 2011; Takada et al., 2014; William Richardson, personal communication). Occasionally, we also observed deletion in the female germline, and so we used a mating of a male Sox10Cre^{0/0};Chrna7^{fl/fl} with a female Sox10Cre⁺⁰;Chrna7^{fl/fl}. We systematically genotyped young mice (P7–8) from toe biopsy with primers to identify each allele in *Chrna7* floxed exon4; deleted exon4; WT exon4. We then excluded all mice in a litter if a deleted exon4 allele was found in any of the pups and stopped the breeding.

'A7flox sens primer' – 'A7flox reverse primer' will amplify a fragment of 369 bp (floxed exon4) or a fragment of 273 bp (WT exon4), the recombinant allele will not be amplified with this primer pair because the sequence recognized by the 'A7flox reverse primer' is deleted. 'A7flox sens primer' – 'a7fd_rev primer' will amplify a fragment of 480bp (deleted exon4). The wild-type (WT) allele is too long (3113 bp) to be amplified by this pair of primers.

a7flox sens: TGCTGAGGCTCAGGGTTTGA
 a7floxrev: CCTTAGGCTTCTCCTCCCCCA
 a7fd_rev: CACGGTGTACAATGGGGAACA

Gene expression profiles

The original RNA sequencing (RNA-seq) files of TSCs (Hastings et al., 2023) and the triceps brachii muscle (Farshadyeganeh et al., 2023) in adult mice were obtained under BioProject IDs of PRJNA922918 and PRJDB16565, respectively. TSCs were defined as NG2+ and S100 β + cells, and were isolated by a fluorescence-activated cell sorter (Hastings et al., 2023). Differential gene expression was analysed by DESeq2 on RNA-seq (Prieto & Barrios, 2020). Normalized values of transcripts per million (TPM) of genes of our interest were also calculated and plotted on a heatmap.

New allele of *ColQ* with deletion of two bases in exon 2 encoding the PRAD domain

We used clustered regularly interspaced short palindromic repeats (CRISPR)/CRISPR-associated protein 9 (Cas9)-based gene editing to generate a novel allele of *ColQ* in which the exon2 sequence has a deletion of 2 bases before the PRAD, the domain required to organize AChE into tetramers. The deletion of two bases has fewer side effects than the insertion of a long fragment of DNA, which we used to generate *ColQ* knockout (KO) mice (Feng et al., 1999). These mice, which do not produce AChE collagen tailed forms in all tissues, including the NMJ, are weaker and smaller than WT. The lethality of these mice during postnatal development was variable, possibly because the temperature of the home cage may have affected development. We used the deleted exon 4 of *Chrna7* as the allele for the KO. We selected to delete *Chrna7* rather than the GABAb1 or GABAb2 receptor in the *ColQ* experiment because the deletion of GABA_B receptors alters the motor function of the mice and thus may negatively affect the activity of *ColQ* independently of its role at the NMJ (Magnaghi et al., 2008).

Quantification mouse activity in the home cage

To quantify the activity of a mouse in a cage, the cage was placed on four force sensors (S_1, S_2, S_3 and S_4), for which force values are recorded at ~ 10 Hz over time (designed by Jean Marc Di Meglio, Professor at Université Paris Cité). This is the principle used by Fowler et al. (2001) and as available from Bioseb (Pinellas Park, FL, USA) and marketed under the name BIO-ACTIV2 ActivMeter, as well as some other commercial setups.

The steps involved in processing the force values to derive an activity/rest signal are shown in Fig. 1 and described below. The sum of the four sensors (i.e. the apparent weight of the mouse over time) is denoted as $(f_t)_{t=1}^n$ where n is the number of samples. If the weight is constant, this means that the mouse is not active (resting); if the weight varies, this means that the mouse is active (regardless of the activity being performed). Over short periods of time, the tare of the balance remains unchanged, but, over long periods of time (day, night), the tare of the balance changes because the activity of the mouse changes the position of the bedding and other objects in the cage. To remove trends induced by these tare drifts, we applied a rolling variance filter, resulting in the signal: $s_t = \frac{1}{300} \sum_{k=t}^{t+299} (f_k - \mu_t)^2$ with $\mu_t = \frac{1}{300} \sum_{k=t}^{t+299} f_k$.

When the mouse is active, the value of the rolling variance can reach or exceed a value of 100. When the mouse is at rest, the signal represents the instrument's background noise for which we assigned a threshold of 1.5.

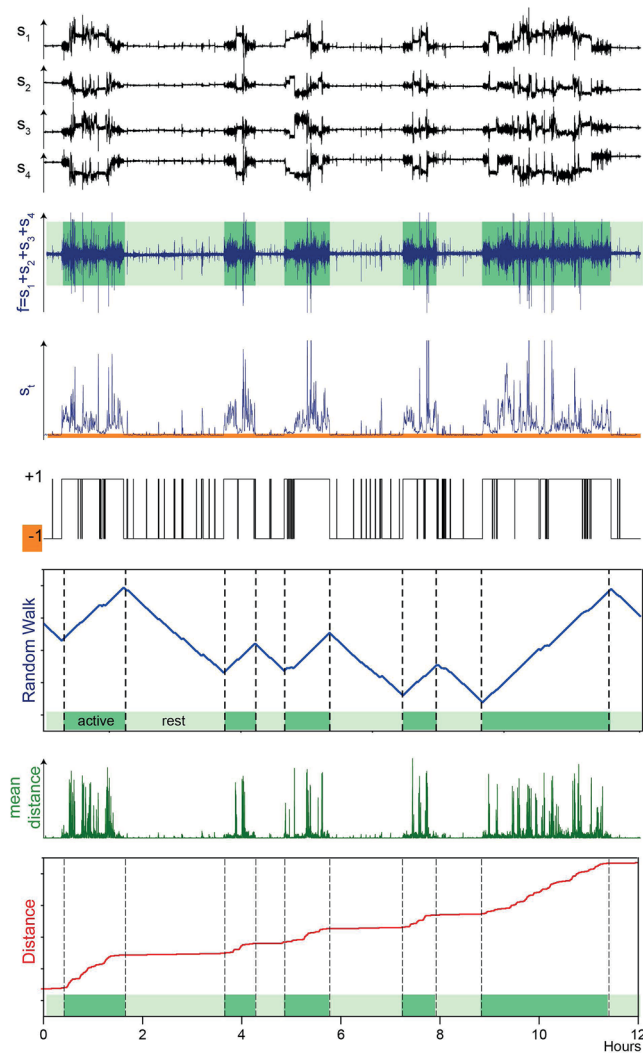


Figure 1. Strategy for quantifying mouse resting time in the breeding cage

The experiment considers an index that distinguishes between mice with different levels of fatigability when in their cage. We expect that mice with greater fatigability will have shorter periods of generalized activity, whatever their activity, defined when the signal from the force sensors rises above a defined threshold. An illustration is provided of the different steps involved in determining the rest and activity periods of a mouse in a breeding cage as described in the Methods. The cage is placed on the four sensors that record the force over time. The signal at the top represents the raw data recorded at 10 Hz for the four sensors S_1 , S_2 , S_3 and S_4 . The sum of the values is shown below. The threshold for activity for the entire recording is obtained by transforming the crude data by the SD (see Methods). If the signal is below the threshold (orange mark), the value is assigned as -1 (rest); if the signal is above, the value is assigned as $+1$. The integration of the data allows us to create a random walk. As described in the text, the automatic segmentation of the cumulative curve assigns its decrease to a rest period; similarly, if the curve increases, the mouse is in an active period. The method describes the automatic segmentation of this curve. In addition, we can know the position of the mouse (see Methods). Because of the translation of the signal, we are not able to calculate the trajectory of the mouse directly, but we are able to derive its average speed

over time and therefore the distance covered during that time, represented by the green curve (see Methods). The integration of this value allows us to calculate the distance travelled during the period represented by the red curve (rest period and active period). [Colour figure can be viewed at wileyonlinelibrary.com]

Thus, when s_t was less than 1.5, we attributed the value -1 to the activity/rest signal; if the value is greater than 1.5, we attributed the value $+1$ to the activity/rest signal. After integration over time, we obtained a random walk plot that increases during periods when the mouse is active and decreases during periods when the mouse is at rest. These variations can be analysed on different time scales, from hours to day–night periods. This activity/rest signal often alternates between activity and rest. To compute robust statistics on the mouse behaviour, the activity/rest signal is smoothed using a change-point detection algorithm (Truong et al., 2020). The chosen method computes the best piecewise constant approximation to the signal of 0 ('rest') and 1 ('activity'). To do this, we apply the segmentation algorithm, the kernel function $k(., .)$ is set to $k(x, y) = x * y$. This kernel change makes the detection method sensitive to changes in the mean value. The only parameter of this method is a threshold that controls the number of changes and is set to 16. In the final signal, very short activities in long rest periods have been smoothed out.

We also calculated the position of the mouse in the cage by applying the conservation of moment law; $x = a^*(S_2 + S_3 - S_1 - S_4)$; $y = b^*(S_2 + S_1 - S_3 - S_4)$, where a and b are constant. To avoid the signal translation, we calculated for each point, a mean tendency of velocity as $\alpha_t^x = \frac{1}{300} \sum_{k=0}^{300} (x_{t+k} - \mu_t^x)(k - \mu^T)$; and $\alpha_t^y = \frac{1}{300} \sum_{k=0}^{300} (y_{t+k} - \mu_t^y)(k - \mu^T)$ where $\mu^T = \frac{1}{301} \sum_{t=0}^{300} t.T$. Then, we calculated the mean arbitrary distance: $d_t = \sqrt{\alpha_t^x + \alpha_t^y}$. After integrating over time, we obtained the arbitrary distance over time for each mouse.

Once the smoothed activity signal is computed for each night and day, we can compute important statistics about the processed signal: the average duration of an activity (or rest) period and the average time spent in an active mode (or inactive mode).

Results

Steps in the regulation of ACh release following activation of the $\alpha 7$ nAChRs at the NMJ

To decipher the signalling pathway that begins with the activation of $\alpha 7$ nAChR by released ACh, we created a robust spillover of ACh by inhibiting AChE and BChE. When AChE is inhibited in the synaptic cleft, the number

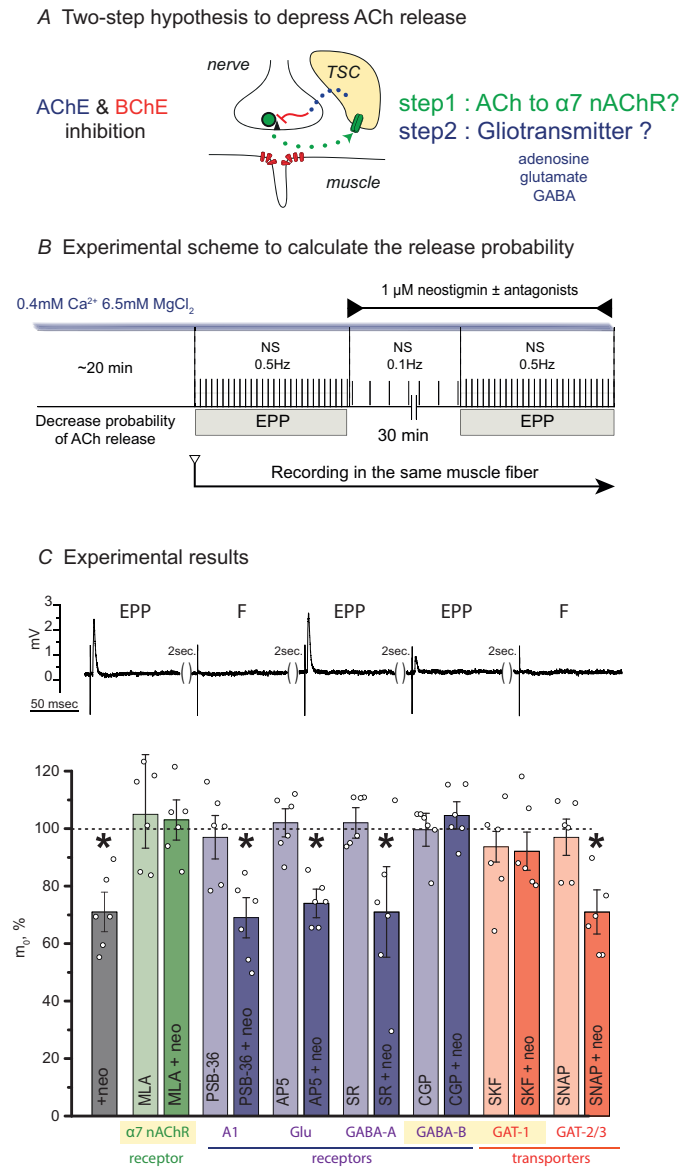


Figure 2. Search for gliotransmitters that could reduce the release of ACh

A, two-step hypothesis: If the ACh released by the nerve activates the $\alpha 7$ nAChR, which is presumably localized on the TSC, the number of vesicles that are subsequently released is reduced. We are looking for a gliotransmitter to explain how the TSC communicates with the nerve terminal. **B**, experimental protocol. If the number of ACh vesicles that are released by the nerve is reduced, we would expect that the probability of release would be reduced as well. The probability of ACh release (m_0) was estimated in low Ca^{2+} (0.4 mM) and high Mg^{2+} (6.5 mM) Krebs–Ringer solution by the method of failures. Under these conditions, the reduced entry of Ca^{2+} ions into the nerve ending means that some fraction of nerve action potentials will not cause the release of ACh quanta (i.e. failure) and, when ACh release does occur, it is limited to one to three quanta. The probability of ACh release in this experimental condition is an index of the efficacy of the release. To allow ACh released from a small number of vesicles, to reach the $\alpha 7$ nAChR on the TSC, we inhibited both AChE and BChE with neostigmine (1 μM). We recorded the number of failures and the EPP in the same muscle fibre in response to 100 motor nerve stimuli at a frequency of 0.5 Hz in the control (before the application of the tested compounds) and 30 min after the application of the tested compounds. The tested compounds were added to the Ringer buffer and the nerve was stimulated at 0.1 Hz during the incubation, with the recording microelectrode left in place. **C**, experimental results: Upper: examples of successive nerve stimulations and recording membrane potential in LAL muscle in the low Ca^{2+} (0.4 mM) and high Mg^{2+} (6.5 mM) Krebs–Ringer solution. EPP, end-plate potentials, and F, ‘failures’, are noted. The empty parenthesis in the original version was an error. Lower: quantification of ACh release probability (m_0) at the NMJs of LAL after incubation with ChE inhibitor neostigmine (neo) and after pre-incubation with $\alpha 7$ nAChRs blocker (MLA, 10 nM), A1 adenosine receptors blocker (PSB-36, 5 nM), glutamate receptor blocker (AP5, 25 μM), GABA_A receptors blocker (SR 95531, 10 μM), GABA_B receptors blocker (CGP 55845, 2 μM), GAT-1 transporter blocker (SKF 89976, 100 μM) and GAT-2/3 transporter blocker (SNAP 5114, 100 μM). Data presented as a percentage of m_0 estimated in the same NMJ before application of the tested compounds. $N = 6$ muscle. * $P < 0.05$ compared to control, paired Student’s t test. [Colour figure can be viewed at wileyonlinelibrary.com]

of released ACh vesicles cannot be calculated by dividing the mean amplitude of full-size EPPs by the mean amplitude of the mEPPs because the zones of action of individual ACh quanta of EPPs on the postsynaptic membrane overlap. As a result, the postsynaptic effect of individual ACh quanta of an EPP is given by their non-linear sum. This process is stochastic and depends on the number of released quanta and the degree of their overlapping (Hartzell et al., 1975). To quantitatively measure the variation in ACh release, we chose the ‘failure’ method to calculate a probability of release by using a solution with low Ca^{2+} and high Mg^{2+} concentrations. This buffer reduces the entry of calcium ions into the nerve terminal at the active zone and limits the neurotransmitter release, such that about half of the nerve stimuli will not trigger the release of an ACh vesicle (failure), and, if ACh release does occur, only one or two vesicles will

be released. In Krebs–Ringer solution with low Ca^{2+} and high Mg^{2+} concentrations, the probability of release (see Methods) is a good indicator of facilitating or inhibiting ACh release. Inhibition of AChE and BChE at the NMJ reduces the probability of ACh release calculated by method of ‘failure’ (Minic et al., 2002). To delineate the steps of this pathway, we calculated the probability of ACh release in the synapses of mouse LAL muscle before and after neostigmine application, a non-specific inhibitor of AChE and BChE. As shown in Fig. 2, the inhibition of cholinesterase (ChE) by neostigmine (1 μM) results in a reduction of $29 \pm 5\%$ ($P = 0.002$) in the probability of ACh release. MLA (10 nM), a specific $\alpha 7$ nAChR antagonist, prevents ($P = 0.52$) the reduction in the probability of ACh release, thereby establishing the first step of this pathway. It has been shown that the activation of $\alpha 7$ nAChRs induced by 50 Hz bursts of nerve stimulation (five trains of 150 pulses applied with a 20 s interburst interval) can

depress ACh release via the activation of A1 adenosine receptors (Noronha-Matos et al., 2020). However, under the experimental conditions employed (low Ca^{2+} and high Mg^{2+} , stimulation at 0.5 Hz), PSB-36 (5 nM), an antagonist of A1 receptors, was unable ($P = 0.003$) to prevent a decrease in the probability of ACh release following inhibition of ChE by neostigmine. We then examined whether other transmitters released by the TSC after activation of $\alpha 7$ nAChRs could reduce the probability of release. Specifically, in addition to ATP and adenosine, glutamate (Colombo & Francolini, 2019) and GABA (Nurullin et al., 2018) have been proposed as gliotransmitters in tripartite neuromuscular synapses.

To test the glutamate hypothesis, we blocked NMDA receptors with AP-5 (25 μM). Inactivation of glutamate receptors did not prevent ($P = 0.008$) the decrease in the probability of ACh release after ChE inhibition with neostigmine (Fig. 2). To test the GABA hypothesis, we blocked either GABA_A receptors with SR-95531 (10 μM) or GABA_B receptors with CGP 55845 (2 μM). Inactivation of GABA_A receptors did not prevent ($P = 0.04$) the effect of neostigmine on ACh release. However, blockade of GABA_B receptors was observed to prevent ($P = 0.26$) the effect of neostigmine on the probability of ACh release (Fig. 2). Therefore, the inhibition of AChE and BChE by neostigmine decreases the probability of ACh release in two steps: first, ACh released from few vesicle activates $\alpha 7$ nAChRs and, second, GABA, presumably gliotransmitter, activates GABA_B receptors on the nerve terminal

In the TSC, Ca^{2+} waves are not necessary for the release of GABA as a gliotransmitter

Gliotransmitter release is often a result of the elevation of intracellular Ca^{2+} levels in TSCs (Araque et al., 2014). This elevation of Ca^{2+} levels by releasing Ca^{2+} from internal stores is a response to motor nerve released neurotransmitters that activate G-coupled proteins on the TSC (Ko & Robitaille, 2015). The activation of $\alpha 7$ nAChRs is also able to induce a phasic Ca^{2+} response in TSC (Noronha-Matos et al., 2020; Petrov et al., 2014). Indeed, continuous stimulation (20 Hz, 120 s) in Krebs–Ringer solution with normal Ca^{2+} level elicited a phasic Ca^{2+} response in TSC that was partially blocked ($P = 0.02$) by the $\alpha 7$ nAChR antagonist MLA (Fig. 3). However, GABA is released following 0.5 Hz frequency nerve stimulation in low Ca^{2+} and high Mg^{2+} buffer. Under these experimental conditions, no significant increase in the Ca^{2+} response in TSC was observed in correlation with the onset of nerve stimulation (Fig. 3). Spontaneous increases in cytoplasmic Ca^{2+} levels were observed to occur infrequently, at a rate of two to three times per minute. The amplitude of these Ca^{2+} oscillations remained unchanged ($P = 0.82$) following the administration of neostigmine (Fig. 3).

Because GABA can be released by a Ca^{2+} independent mechanism, we investigated whether GABA can be released by GAT in the reverse mode (i.e. GAT can release GABA depending on the internal sodium ion concentration and membrane depolarization) (Palacín et al., 1998). To test the GAT hypothesis, we blocked either

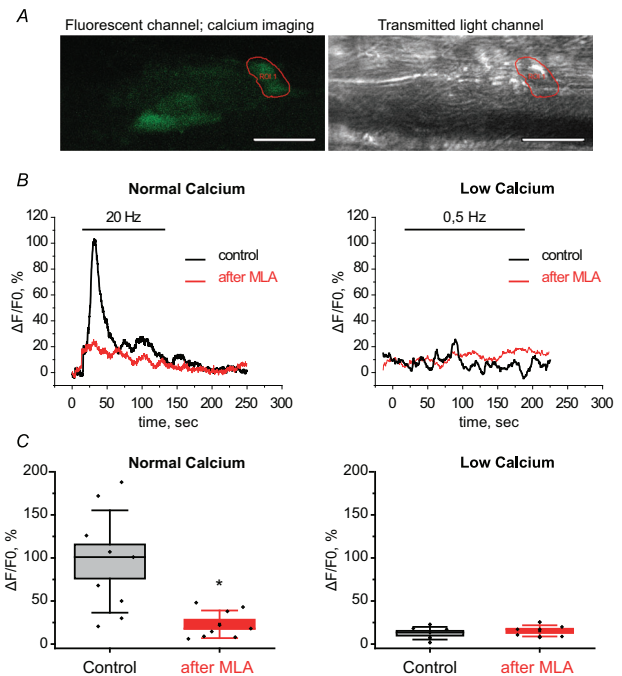


Figure 3. An $\alpha 7$ nAChR-mediated oscillatory Ca^{2+} response in TSC of LAL muscle

Continuous motor nerve stimulation (20 Hz, 120 s) in Krebs–Ringer solution with normal Ca^{2+} levels elicited a phasic Ca^{2+} response in TSC. These oscillatory Ca^{2+} responses were partially blocked by the $\alpha 7$ nAChRs blocker (MLA, 10 nM). However, at 0.5 Hz frequency of nerve stimulation with low Ca^{2+} and high Mg^{2+} levels in Krebs–Ringer solution, no significant increase in the Ca^{2+} responses in TSC was observed with the onset of nerve stimulation. Spontaneous increases in cytoplasmic Ca^{2+} levels were observed to occur infrequently, at a rate of two or three times per minute. The amplitude of these Ca^{2+} oscillations remained unchanged after neostigmine administration. **A**, locating a region of interest (ROI). Image of a fluorescence channel (left) and a transmitted light channel (right) of confocal microscope with TSC as a ROI. **B**, experimental data: evolution of Ca^{2+} signal over time. Left panel, example of Ca^{2+} responses elicited in the same TSC of LAL muscle in Krebs–Ringer solution with normal Ca^{2+} level before (black line) and after $\alpha 7$ nAChRs blocker (MLA, 10 nM) (red line). Right: example of Ca^{2+} responses elicited in TSC of LAL muscle in the low calcium (0.4 mM) high magnesium (6.5 mM) Krebs–Ringer solution before (black line) and after treatment with neostigmine (red line). **C**, quantification of the Ca^{2+} signal. Left: quantification of Ca^{2+} responses in TSC of LAL muscle in Krebs–Ringer solution with normal Ca^{2+} level before and after $\alpha 7$ nAChRs blocker (MLA, 10 nM) ($N = 9$ muscles). Right: quantification of Ca^{2+} responses elicited in TSC of LAL muscle in the low Ca^{2+} (0.4 mM) high Mg^{2+} (6.5 mM) Krebs–Ringer solution before and after neostigmine treatment ($N = 6$ muscles). * $P < 0.05$ compared to control, Mann–Whitney test. [Colour figure can be viewed at wileyonlinelibrary.com]

GAT-1 with SKF89976-A (100 μM) or GAT-2/GAT-3 with SNAP 5114 (100 μM). As shown in Fig. 2 SKF89976-A (GAT-1 blocker) ($P = 0.36$) but not SNAP 5114 (GAT-2/GAT-3 blocker) ($P = 0.005$) prevented the effect of neostigmine.

Taken together, these data suggest a novel pathway: ACh that escapes AChE and BChE activates $\alpha 7$ nAChRs on the TSC, which then triggers GABA release by reversion of GAT-1 transporter; GABA released from TSC then activates the GABA_B receptor and depresses the release of ACh, presumably by regulating voltage-gated calcium channels located at the active zone.

TSC in the NMJ can express genes mediating GABA synthesis and release

Immunofluorescence visualization. The presence of all key components of this regulatory pathway at the NMJ of the mouse LAL was also supported by immunohistochemistry. The $\alpha 7$ nAChRs, GABA, GABA_B receptors and GAT-1 were labelled at the NMJ area using specific antibodies (Fig. 4A).

Gene expression profiles. To complement this immunological analysis, we performed a comprehensive gene expression profile of TSCs and triceps brachii muscle in adult mice. We found that BChE and *Prima1*, which are markers of TSCs, were indeed enriched in TSCs (Fig. 4B and Table 1). Similarly, $\alpha 7$ nAChR (*Chrna7*), which interacts with ACh spillover, was also enriched in TSCs, but its expression level appeared to be much lower. Glutamate decarboxylases (*Gad1* and *Gad2*) and membrane GATs (*Best1*, *Slc6a1*, *Slc6a11* and *Slc6a12*) were also enriched in TSCs, although no statistical significance was observed for *Best1* or *Slc6a12*. The vesicular GAT (*Slc32a1*) has a very low abundance and is enriched in TSCs compared to muscle, but the statistical significance could not be calculated because it is so close to zero.

GABA depresses the quantal content when BChE is inhibited at the NMJ

To further characterize the $\alpha 7$ /GABA_B receptor-mediated pathway, we calculated the number of ACh vesicles released (quantal content) before and after inhibition of BChE when AChE is fully active at mouse diaphragm NMJs as described in Fig. 5A and as previously reported (Petrov et al., 2014). Because BChE is not present in the synaptic cleft, the quantal content can be calculated directly by dividing the mean amplitude of the EPPs by the mean amplitude of the mEPPs. Bath application of iso-OMPA (50 μM), a specific BChE inhibitor, significantly decreased ($P = 0.003$) the mean quantal content of EPPs by $19 \pm 5\%$ (Fig. 5B). This effect of iso-OMPA was pre-

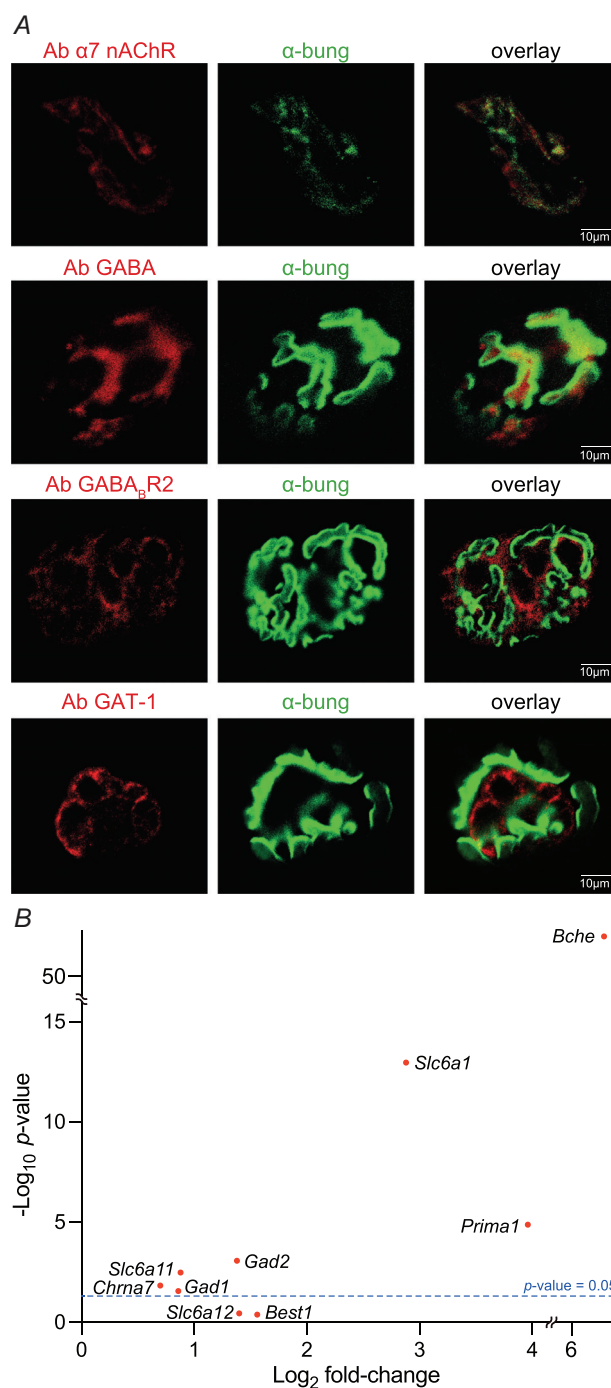
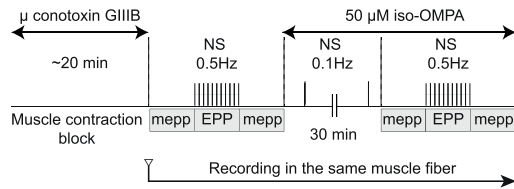
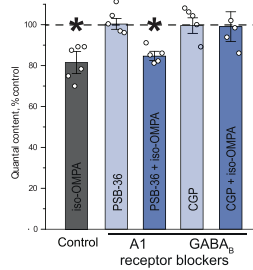


Figure 4. Identification of molecular actor at the NMJ
 A, immunostaining for $\alpha 7$ nAChRs, GABA, GABA_B receptors and GAT-1 at the NMJs of the mouse levator auris longus (LAL). Muscles were incubated with the antibodies (red labelling) directed against $\alpha 7$ nAChR (first panel), GABA (second panel), R2 subunit of GABA_B receptor (third panel) and GAT-1 transporter of GABA (fourth panel). The NMJs were identified with labelled α -bungarotoxin (green labelling). B, RNA-seq analysis. Scatter plot of log₂ of fold-change (TSCs/muscle) and $-\log_{10}$ of the *P* value of genes of our interest based on RNA-seq of triplicated triceps brachii muscle and sextuplicated TSCs in adult mice. The fold-change of *Slc32a1* is infinity, and is not plotted. For differential gene expression, see Table 1. [Colour figure can be viewed at wileyonlinelibrary.com]

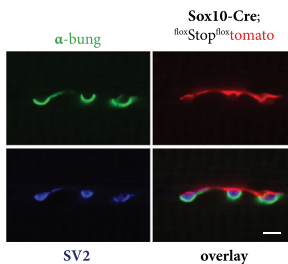
A Experimental scheme to calculate QC



B Quantification QC



C At NMJ, Sox10-Cre acts in TSC



D Quantification QC

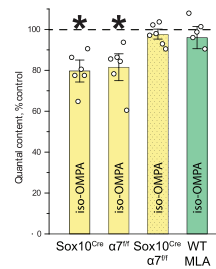


Figure 5. The α7/GABA_B receptor-mediated pathway reduces the quantal content of EPP in the diaphragm of WT mice when BChE is inhibited

To confirm the characteristics of the α7/GABA_B receptor pathway, we directly calculated the number of vesicles released in the diaphragm muscle. To allow ACh that escapes from AChE clustered in the synaptic cleft (spillover) to reach the α7 nAChR on the TSC covered by BChE, we inhibited BChE with iso-OMPA (50 μM). A, experimental protocol. Diaphragm muscle contraction was blocked by inhibition of the muscle voltage-gated sodium channels with μ-conotoxin GIIIB. A sharp microelectrode was inserted close to a NMJ to record focal mEPPs and EPPs. A first recording was obtained for the mEPPs (no nerve stimulation), a second for EPPs (0.5 Hz nerve stimulations) and a third for the mEPPs (no stimulation). BChE inhibitor (iso-OMPA, 50 μM), A1 adenosine receptor blocker (PSB-36, 5 nM) or GABA_B receptor blocker (CGP 55845, 2 μM) were added to the Ringer buffer and the nerve was stimulated at 0.1 Hz during the incubation. The recording microelectrode was maintained in place. All recording were obtained in 30–40 min. The quantal content was obtained by dividing the mean amplitude of the EPPs by the mean amplitude of the mEPPs. B, quantification of quantal content (QC). The effect of BChE inhibition on quantal content of EPP after pre-incubation with A1 adenosine receptor blocker (PSB-36, 5 nM) or GABA_B receptor blocker (CGP 55845, 2 μM). Inhibition of BChE with iso-OMPA (50 μM) did not reduce the quantal content when GABA_B receptors were blocked. Data are presented as a percentage of quantal content estimated in the same NMJ before application of iso-OMPA and receptor blockers. N = 5 muscles. *P < 0.05 compared to control, paired Student's t test. C, tissue-specific

Table 1. Differential expressions of genes of interest.

Gene	Triceps brachii muscle (TPM)	TSCs (TPM)	log ₂ FC	Adjusted P value
<i>Bche</i>	1.341	180.689	6.28	3.31 × 10 ^{-50*}
<i>Prima1</i>	1.603	39.455	3.96	1.36 × 10 ^{-5*}
<i>Chrna7</i>	0.003	0.630	0.70	1.47 × 10 ^{-2*}
<i>Gad1</i>	0.008	0.826	0.86	2.81 × 10 ^{-2*}
<i>Gad2</i>	0.007	1.616	1.38	8.59 × 10 ^{-4*}
<i>Best1</i>	0.163	2.429	1.56	4.21 × 10 ⁻¹
<i>Slc6a1</i>	0.093	7.046	2.88	1.12 × 10 ^{-13*}
<i>Slc6a11</i>	0.008	0.849	0.88	3.28 × 10 ^{-3*}
<i>Slc6a12</i>	0.100	1.908	1.40	3.57 × 10 ⁻¹
<i>Slc32a1</i>	0.000	0.009	∞	Not available

TPM, transcripts per million. FC, fold-change (TSCs/muscle). *Adjusted P < 0.05. Because *Slc32a1* was not expressed at all in the triceps brachii muscle, the P value could not be calculated.

expression of SOX10-Cre in the TSC. The reporter genes Tomato (a cytoplasm-soluble red fluorescent protein) is highly expressed in the TSC, but not in muscle fibres or in the nerve. The endplate area was identified with labelled α-bungarotoxin (α-Bung). The nerve ending was identified with labelled vesicular ACh transporter (vAChT) and synaptophysin (SV2) (N = 6 muscles, 10 NMJ). D, quantification of quantal content (QC). Quantification of the quantal content of EPP after inhibition of BChE in diaphragm muscle of WT mice and mutants with specific deletion of α7 nAChRs in TSCs. Inhibition of BChE with iso-OMPA (50 μM) did not reduce the quantal content in mice lacking α7 nAChRs in TSCs. Data presented as percentage of quantal content estimated in the same NMJ before application of iso-OMPA. N = 6 muscles. *P < 0.05 compared to control, paired Student's t test. [Colour figure can be viewed at wileyonlinelibrary.com]

vented (P = 0.53) by pretreatment with an α7 nAChRs blocker (MLA, 10 nM), as previously reported (Petrov et al., 2014). To further evaluate the second step, we examined the effects of a GABA_B receptor blocker (CGP 55845, 2 μM) and an A1 receptor antagonist (PSB-36, 5 nM) when BChE was inhibited but AChE fully active. CGP 55845 (P = 0.95) but not PSB-36 (P = 0.001) prevented the effect of iso-OMPA on the quantal content of EPPs (Fig. 5B). Thus, inhibition of BChE located on TSC allows ACh non-hydrolysed by synaptic AChE to reach α7 nAChRs and then trigger the α7/GABA_B receptor-mediated pathway.

Genetic deletion of α7 nAChR in TSC prevents the effect of BChE inhibition on ACh release

To confirm that α7 nAChRs localized on the surface of TSCs initiate activation of the α7/GABA_B

receptor-mediated pathway, we next used a genetic approach to specifically eliminate the $\alpha 7$ nAChR in Schwann cells, but not in motoneurons or muscle fibres. We used an allele of *Chrna7* with a floxed exon 4, because deletion of *Chrna7* exon 4 by the recombinase Cre kills $\alpha 7$ nAChR (Hernandez et al., 2014). To delete floxed *Chrna7* in Schwann cells but not in nerve or muscle, we used a mouse expressing Cre under the *Sox10* promoter (Matsuoka et al., 2005). To confirm the expression of SOX10-Cre in the TSC but not in muscle fibre or nerve, we used two reporter genes: Tomato: a cytoplasm-soluble red fluorescent protein (Fig. 5C) or Channel rhodopsin (CHR2-EYFP), a membrane protein fused to YFP (not shown). Both reporter genes are highly expressed in the TSC at the level of the NMJ, but not in the muscle fibres or in the nerve. In *Sox10-cre^{+ / 0}; Chrna7^{flox / flox}* mice ($P = 0.27$) but not in *Sox10-cre^{+ / 0}* mice ($P = 0.003$) or in *Chrna7^{flox / flox}* mice ($P = 0.01$), inhibition of BChE with iso-OMPA does not decrease the quantal content as shown in Fig. 5D. Thus, it can be concluded that specific BChE inhibition decreases ACh release via activation of $\alpha 7$ nAChRs on TSCs.

Activation of the $\alpha 7$ /GABA_B receptor-mediated pathway when ChEs are active

In the previous experiments, we stimulated the nerve at low frequency and we used BChE inhibitor. BChE concentrated on the surface of the TSC hydrolyses ACh that escapes AChE in the synaptic cleft before it can activate $\alpha 7$ nAChRs and induce TSC GABA release. Does this negative regulatory loop occur under normal conditions when ChEs are fully active? It is well known that the amplitude of the EPP decreases when the frequency of the nerve discharge increases. It is thus conceivable that part of the reduction of EPP amplitude could be a consequence of activation of $\alpha 7$ nAChRs on the TSC by ACh not hydrolysed during repetitive discharge. Therefore, we recorded EPPs in the mouse diaphragm during trains of 50 repetitive motor nerve stimulations at 10, 20, 50 and 70 Hz, under normal conditions and in the presence of a GABA_B receptors blocker (CGP 55845, 2 μ M). As shown in Fig. 6A, the relative decrement of EPP amplitude (i.e. the reduction of EPP amplitude normalized to the first) is similar when GABA_B receptors are functional or blocked. Indeed, in normal mice, the decrease in EPP amplitude during short bursts of stimulation does not depend on the $\alpha 7$ /GABA_B receptor-mediated pathway.

To further increase ACh spillover, we applied long trains of repetitive motor nerve stimulations (20 Hz, 120 s), which are known to elicit an $\alpha 7$ nAChR-mediated oscillatory Ca²⁺ response in TSC (Fig. 3) and we evaluated whether the $\alpha 7$ /GABA_B receptor-mediated

pathway altered the quantal content of EPP. To calculate the quantal content of the EPP, we recorded mEPPs and EPPs at 0.5 Hz of nerve stimulation in mouse LAL muscle before and after a tetanic nerve stimulation (20 Hz, 120 s), as presented in Fig. 6B. The quantal content of the EPP decreased significantly ($P = 0.02$) to $83 \pm 5\%$ of the control level after a tetanic nerve stimulation (Fig. 6B). To evaluate whether GABA is responsible for this depression, the muscles were incubated with CGP 55845 (2 μ M) for 30 min, the quantal content was calculated, then the tetanic nerve stimulation (20 Hz, 120 s) was applied, and the quantal content was calculated (Fig. 6B). CGP 55845 completely prevented ($P = 0.31$) development of post-tetanic depression of ACh release, supporting the idea that GABA released by the TSC is the relevant gliotransmitter. To evaluate whether the activation of $\alpha 7$ nAChR receptor is responsible for the depression, the muscles were incubated in MLA (10 nM) for 30 min, the quantal content was calculated, then the tetanic nerve stimulation (20 Hz, 120 s) was applied, and the quantal content was recalculated. The quantal content of the EPP increased significantly ($P = 0.04$) to $131 \pm 13\%$, after the tetanic nerve stimulation (Fig. 6B). Thus, activation of the $\alpha 7$ nAChR receptor is a key step of the depression, among other mechanisms which contribute to the post-tetanic potentiation.

Together, these data suggest that activation of this $\alpha 7$ /GABA_B receptor-mediated pathway depends on the amount of ACh that escapes both from clustered AChE in the synaptic cleft and from PRiMA-anchored BChE on the TSC to activate $\alpha 7$ nAChRs on the TSC. To further explore the relevance of this $\alpha 7$ /GABA_B receptor-mediated pathway, we examined two conditions under which AChE is reduced at the NMJ and, thus, in very young mice during the postnatal development, and under a pathological condition when AChE is not clustered in the basal lamina as a result of mutation of the *ColQ* gene.

The $\alpha 7$ /GABA_B receptor-mediated pathway depresses ACh release at the NMJs of newborn mice

During early postnatal development, the initially low level of muscle AChE increases (Lomo, 2003) and the morphology of the NMJs changes (Sanes & Lichtman, 1999). We examined whether spillover of ACh from immature nerve muscle during this period may activate the $\alpha 7$ /GABA_B receptor-mediated pathway, if this pathway is already functional.

First, we compared changes in the level of AChE, labelled with fluorescent Fasciculin-2 at the NMJ in diaphragm muscle between newborn and adult mice. (Fig. 7A). At P0 and P1, AChE was not detected at the NMJs (Table 2). The significantly lower level of AChE

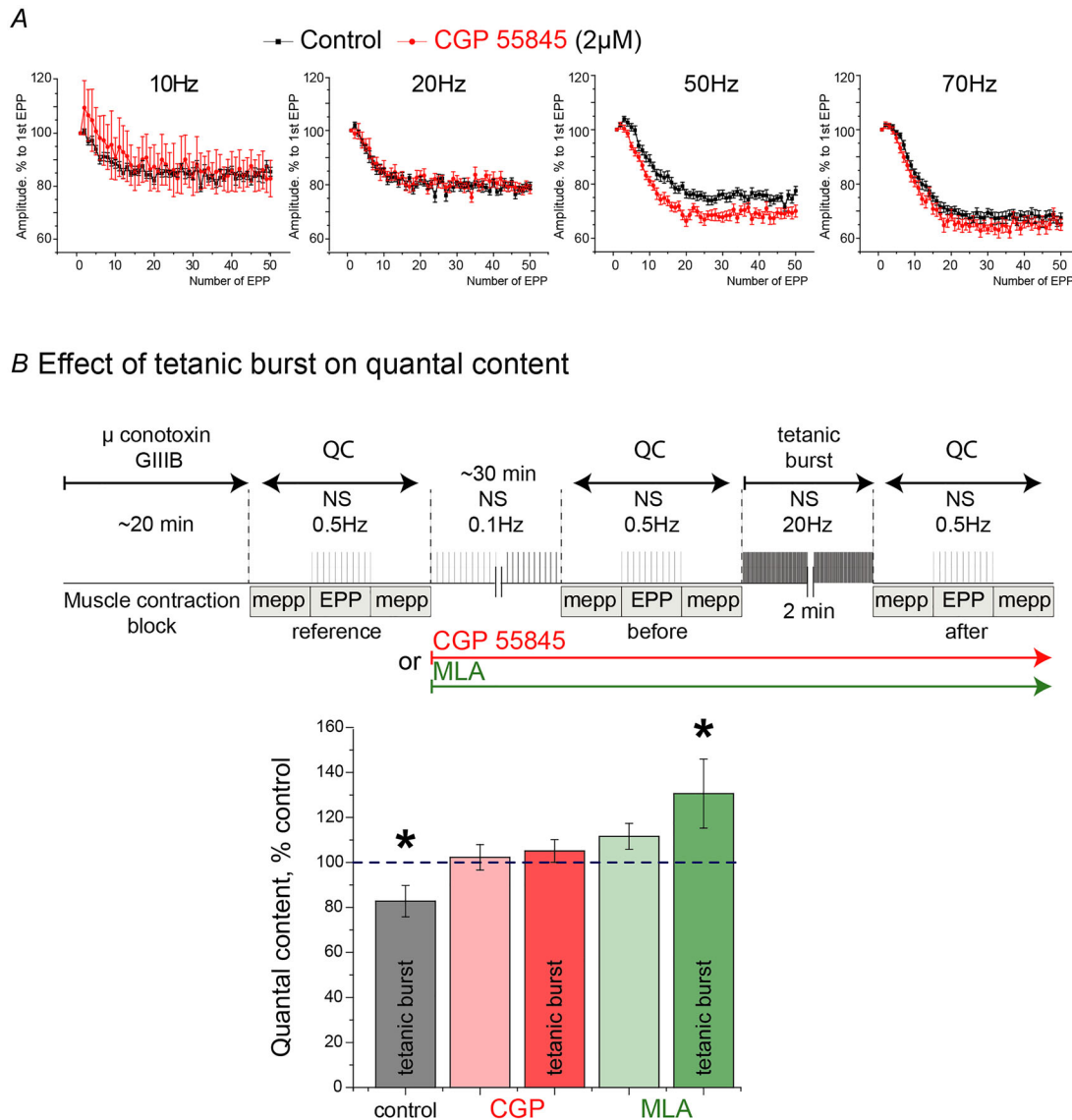


Figure 6. With fully active ChE, the $\alpha 7$ /GABA_B receptor-mediated pathway decreases ACh release under extreme circumstances

To evaluate how this pathway contributes to the normal NMJ, we analysed the consequences of short burst nerve discharges or the consequences after long tetanic stimulation. *A*, bursts of nerve discharges change the amplitudes of the EPP independent of the $\alpha 7$ /GABA_B receptor-mediated pathway. Quantification of the effect of inhibition of GABA_B receptors on the decrement of EPP amplitudes. The motor nerve was stimulated at a frequency of 10, 20, 50 and 70 Hz (50 stimuli), with 1 min of rest between each set of stimuli. In each muscle, as a control, recordings were made in five or six NMJs before application of GABA_B receptor blocker. The tested compound was then applied for 30 min, after which recordings were made in another set of five or six NMJs using the same stimulation protocol. Data are presented as a percentage of EPP amplitude during the train compared to the amplitude of the first EPP. *N* = 25–30 NMJs from five muscles. *B*, tetanic stimulation activates the $\alpha 7$ /GABA_B receptor-mediated pathway. The upper part shows the experimental scheme to calculate the quantal content (QC) of EPP. QC was calculated repeatedly, before incubation with $\alpha 7$ nAChRs blocker (MLA, 10 nM) or GABA_B receptor blocker (CGP 55845, 2 μ M), before tetanic stimulation and after tetanic stimulation. The lower part shows the variation of quantal content before and after tetanic stimulations. Under the control condition, the quantal content decreased to 83%, whereas, when GABA_B or $\alpha 7$ nAChRs receptors are blocked, QC is not reduced. [Colour figure can be viewed at wileyonlinelibrary.com]

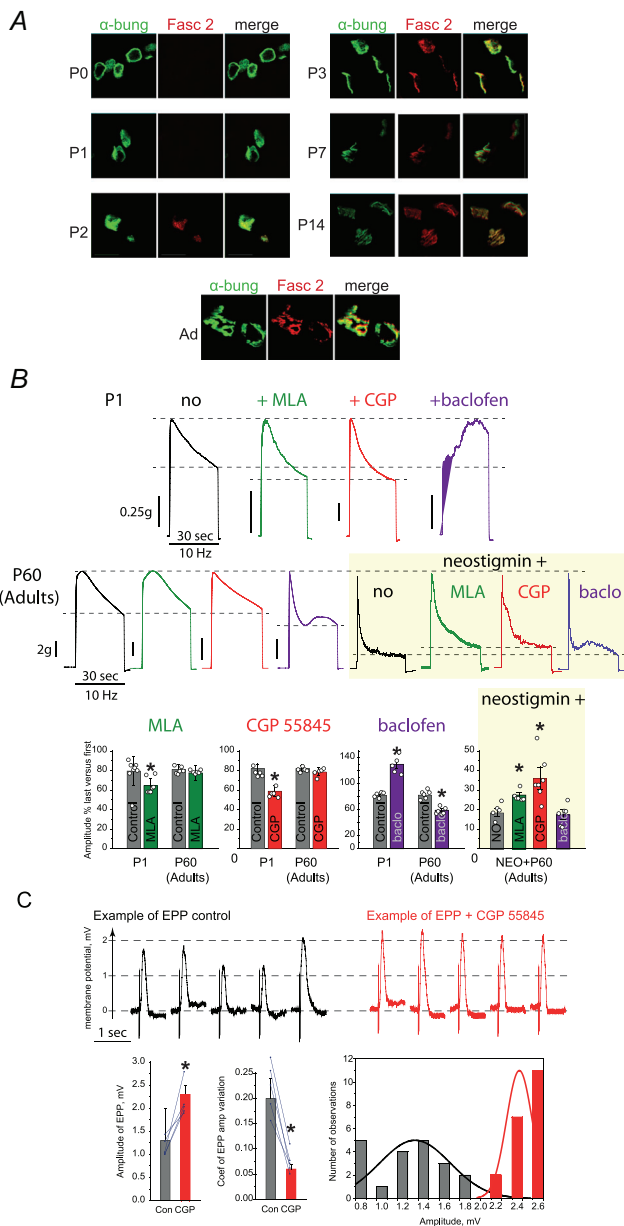


Figure 7. The $\alpha 7$ /GABA_B receptor-mediated pathway reduces ACh release in diaphragm muscle of newborn mice

A, quantification of AChE with fluorescent Fasciculin-2. Labelling of synaptic AChE with red fluorescent Fasciculin-2 (Fasc 2) in the diaphragm muscle of newborn (P0–14) and adult (Ad) mice. The endplate area was identified with green labelled α -bungarotoxin (α -bung). B, diaphragm fatigue. Upper: representative contractions of diaphragm muscle of newborn (P1) and adult (P60) mice during a 30 s train of motor nerve stimulation at the frequency of 10 Hz. Lower: quantification of the relative changes of contraction force during the train (10 Hz, 30 s) in control and in the presence of $\alpha 7$ nAChRs blocker (MLA, 10 nM), GABA_B receptor blocker (CGP 55845, 2 μ M), agonist of GABA_B receptor (Baclofen) and cholinesterases inhibitor neostigmine (1 μ M). Data are presented as a percentage of the force of the last contraction during the tetanus compared to the force of the first contraction. $N = 5$ muscles. $*P < 0.05$ compared to control, Mann–Whitney test. C, EPP properties recorded in P2 mouse diaphragm. Upper: example of EPP trace recorded before and after

incubation with GABA_B receptor blocker (CGP 55845, 2 μ M). Lower: mean of EPP parameters (amplitude, coefficient of variation of EPP amplitude) before black or red after GABA_B receptor blocker (CGP 55845, 2 μ M). An example of changes in the number of EPP with different amplitudes during the experiment is shown on the right. [Colour figure can be viewed at wileyonlinelibrary.com]

Table 2. Quantification of AChE level by Fas-Alexa647 at the NMJ of newborn and adult mice.

Age	Level of Alexa fluorescence per μm^2	P compared to adults (Mann–Whitney test)
Adults (P60)	124 \pm 8	–
P0	Not identified	–
P1	Not identified	–
P2	88 \pm 12*	0.04
P3	86 \pm 9*	0.03
P7	94 \pm 10	0.07
P14	113 \pm 13	0.15

* $P < 0.05$ (Mann–Whitney test).

compared to adult mice was detected at the ages of P2 ($P = 0.04$) and P3 ($P = 0.03$) (Table 2). From P7 ($P = 0.07$) to P14 ($P = 0.15$), AChE levels were not significantly different from those of adult animals.

As a second step, to challenge synaptic transmission in neonatal mice, we stimulated the nerve at 10 Hz for 30 s, as proposed by Heredia et al. (2016) and recorded the maximal force before and after application of the $\alpha 7$ nAChR blocker MLA (10 nM), the GABA_B receptor blocker CGP 55845 (2 μ M) and the GABA_B receptor agonist baclofen (100 μ M) (Fig. 7B). The stimulation train at 10 Hz for 30 s induced muscle fatigue, calculated as the ratio of the last and first contraction in the train (Fig. 7B). In newborn mice (P1), the force of the last contraction before and after application of MLA or CGP 55845 decreased from 80 \pm 5% to 64 \pm 3% ($P = 0.02$) and to 59 \pm 3% ($P = 0.01$), respectively (Fig. 7B). Conversely, activation of GABA_B receptors by baclofen increased muscle force in newborn mice. The force of the last contraction increased significantly from 82 \pm 2% in control to 130 \pm 6% ($P = 0.01$) after incubation of the muscles with baclofen (Fig. 7B).

Third, we performed *ex vivo* electrophysiological experiments to verify that activation of GABA_B receptors by endogenous GABA can affect ACh release during early postnatal development. EPPs were recorded in mouse diaphragm muscles of mice at the age of P2. Low calcium (0.1 mM) and high magnesium (8.0 mM) Krebs–Ringer solution was used to block diaphragm muscle contractions by reducing ACh release. In the same muscle fibre, 20 EPPs were recorded before (control) and after 20 min of CGP 55845 (2 μ M) application. For each experiment, the mean, SD and CV of the EPP amplitudes were calculated (del

Castillo & Katz, 1954). After application of CGP 55845, the mean amplitude of the EPP increased by 1.7 times: from 1.3 ± 0.07 mV in control to 2.3 ± 0.2 mV ($P = 0.02$) after incubation with CGP 55845 (Fig. 7C). As a result, the mean CV significantly decreased by a factor of 3.4: from 0.2 ± 0.04 in control to 0.06 ± 0.01 ($P = 0.03$) after incubation with CGP 55845 (Fig. 7C). Thus, activation of GABA_B receptors by endogenous GABA decreases ACh release during early postnatal development.

By contrast to newborn mice, MLA or CGP 55845 did not affect fatigue in adult mice (P60) during the same stimulus protocol as above (10 Hz for 30 s). This may be because ACh released from the nerve during this stimulation pattern does not reach the $\alpha 7$ nAChR on the TSC in the mature NMJ. Alternatively, released ACh activates the $\alpha 7$ /GABA_B receptor-mediated pathway but does not reduce the size of the EPP below the threshold for action potential generation. However, in adults, baclofen application significantly increased muscle fatigue, with the mean force of the last contraction in the train decreasing from $83 \pm 3\%$ to $59 \pm 2\%$ ($P = 0.005$). This may be because activation of the GABA_B receptor on the nerve terminal decreases ACh release and reduces the size of the EPP below the threshold for action potential generation.

To increase the potential activation of $\alpha 7$ nAChR on the TSC of adult mice, AChE and BChE were inhibited with neostigmine (1 μ M). This significantly increased diaphragm muscle fatigue, calculated as the ratio of the last and first contraction in the train (10 Hz for 30 s). The force of the last contraction decreased from $80 \pm 6\%$ in control to $20 \pm 4\%$ ($P = 0.01$) after application of neostigmine (Fig. 7B). This may be explained by the drop of EPP amplitude below threshold for the generation of a muscle action potential, as previously reported (Petrov et al., 2014). Preincubation of muscle with MLA or CGP 55845 significantly reduced the effect of neostigmine on muscle fatigue from $20 \pm 4\%$ (in neostigmine alone) to $27 \pm 3\%$ ($P = 0.01$) and $34 \pm 12\%$ ($P = 0.007$), respectively (Fig. 7B). It should be noted that, in adult mice, after the increase in muscle fatigue caused by application baclofen, neostigmine did not have a fully additive effect (Fig. 7B). After pre-activation of GABA_B receptors with baclofen, the force of the last contraction decreased from $59 \pm 6\%$ (in baclofen) to $18 \pm 5\%$ ($P = 0.008$) (in neostigmine). The effect of neostigmine after baclofen is not significantly different ($P = 0.23$) from the effect of neostigmine itself.

The lack of an additive effect of baclofen and neostigmine is also consistent with the idea that part of the effect of neostigmine is mediated by the activation of GABA_B receptors. However, it cannot be ruled out that there are other mechanisms by which ChE inhibition may reduce the force of muscle contractions.

The $\alpha 7$ /GABA_B receptor-mediated pathway can be activated in mice with end-plate AChE deficiency

ACh spillover can also be significant when AChE is not clustered at the NMJ by ColQ. Mutations in ColQ are responsible for a congenital myasthenic syndrome that shows an AChE deficit at the NMJ (Ohno et al., 2000). The AChE deficit and the ColQ protein deficit induce profound postsynaptic remodeling (Sigoillot et al., 2016). In addition, ACh may escape the synaptic cleft and activate the $\alpha 7$ /GABA_B receptor-mediated pathway, despite the localization of BChE anchored by PRiMA on the TSC. Therefore, the release of ACh may be depressed during repetitive activities and may contribute to fatigue during exercise. To test this hypothesis, we studied the consequences of blocking this regulatory loop on EPP amplitude *ex vivo*, and on the natural activity of mice activity in their home cages *in vivo*.

Electrophysiology at the NMJ in the diaphragm of WT and mice and ColQ^{-/-} mutant mice revealed no significant change in the mean amplitude of EPPs at 0.5 Hz nerve stimulation when the NMJ is adapted to AChE deficiency (Fig. 8B). At a low frequency of motor nerve stimulation, CGP 55845 (2 μ M) did not significantly change ($P = 0.71$) the mean amplitude of EPP (Fig. 8B). However, at higher nerve stimulation frequencies, EPP amplitude decreased more rapidly in ColQ^{-/-} mutant muscles than in control muscles (Fig. 8C). In WT, stimulation frequencies of 10, 30 or 50 Hz all result in an $\sim 20\%$ decrease in EPP amplitude after about eight stimuli. ColQ^{-/-} mutant muscles were able to maintain EPP amplitudes with a decrement similar to that of controls at 10 Hz (20% decrement), but rapidly decreased to $\sim 40\%$ and 65% of initial values at 30 and 50 Hz, respectively. CGP 55845 (2 μ M) had the opposite effect on the decrement of EPP amplitudes, depending on the stimulation frequency (Fig. 8C). At 30 Hz of nerve stimulation, CGP 55845 maintained EPP amplitudes close to the EPP amplitude of WT muscles (Fig. 8C). By contrast, at 50 Hz, CGP 55845 significantly accentuated the reduction of EPP amplitudes (Fig. 8C). This reduction occurred after four or five stimulations, whereas, during the second and third stimulation, the amplitude of the EPP after CGP 55845 was higher than in the control. This suggests that the excess ACh release at 50 HZ that occurs after blockade of the $\alpha 7$ /GABA_B receptor-mediated pathway reduces the amplitude of the EPP by another mechanism, possibly through desensitization of nAChRs. Thus, the $\alpha 7$ /GABA_B receptor-mediated pathway can be activated by endogenous ACh under pathological conditions when AChE is not concentrated at the NMJs as a result of mutation in the ColQ gene and BChE is active at the TSC.

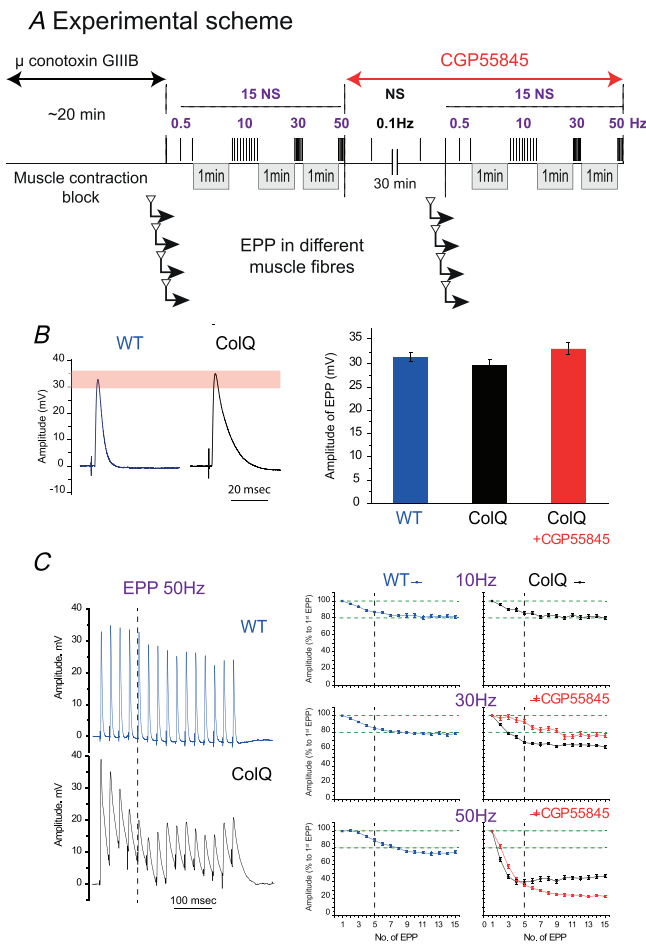


Figure 8. The $\alpha 7$ /GABA_B receptor-mediated pathway can be activated by endogenous ACh when AChE is absent at the NMJs as a result of mutation in the ColQ gene

A, experimental protocol. Diaphragm muscle contraction was blocked by μ -conotoxin GIIIB. A sharp microelectrode was inserted near a NMJ to record EPPs. The motor nerve was stimulated at a frequency of 0.5, 10, 20, 50 and 70 Hz (15 stimuli) with 1 min of rest between each set of stimuli. In each muscle, recordings were made at five or six NMJs before application of GABA_B receptors blocker. These data were used as a control. Then GABA_B receptor blocker was applied for 30 min, after which recordings were made in another five or six NMJs using the same stimulation protocol. **B**, properties of single EPP. Left: representative EPPs recorded in the diaphragm muscle of WT mice and *ColQ*^{-/-} mice with endplate AChE deficiency when the motor nerve was stimulated at a frequency of 0.5 Hz. Right: quantification of the mean amplitude of EPPs at 0.5 Hz nerve stimulation before and after application of the GABA_B receptors blocker (CGP 55845, 2 μ M). **C**, quantification on the decrement of EPP amplitudes at high frequency nerve stimulations. Left: representative EPPs recorded in diaphragm muscle of WT mice and *ColQ*^{-/-} mice when the motor nerve was stimulated at a frequency of 50 Hz. Right: quantification of the decrease in amplitudes of EPPs in diaphragm of WT and *ColQ*^{-/-} mutant mice during high frequency of nerve stimulation. Quantification of the successive EPPs at 10, 30 or 50 Hz nerve stimulation before (black) and after (red) application of the GABA_B receptors blocker (CGP 55845, 2 μ M). Data are presented as percentage of EPP amplitude during the train compared to the amplitude of the first EPP. *N* = 25–30 NMJs from five muscles. [Colour figure can be viewed at wileyonlinelibrary.com]

To determine whether the $\alpha 7$ /GABA_B receptor-mediated pathway affects the behaviour of *ColQ*^{-/-} mice, we used a genetic approach to knock out the $\alpha 7$ /GABA_B receptor-mediated pathway in *ColQ* mice. We chose to invalidate the $\alpha 7$ nAChR rather than the GABA_B receptor because *Chrna7*^{-/-} mice have a normal motor function, whereas *Gabbr1* or *Gabbr2* mice have a severe phenotype. *ColQ*^{-/-} mice and the double mutant *Chrna7*^{-/-};*ColQ*^{-/-} mice are significantly smaller than WT, and both mouse strains were affected by severe muscle weakness. Although a control mouse was able to hold on to a grid (inverted screen test), mice of both genotypes were unable to do so, and fell immediately. On the other hand, direct observation of these two strains revealed a different motricity. Although *ColQ*^{-/-} mice stopped quickly when handled, *Chrna7*^{-/-};*ColQ*^{-/-} mice moved more confidently.

These differences are difficult to quantify because they depend on several parameters, including the period of the experiment (time of day, awake state), interaction with the experimenter and stress. Mice have different individual behaviours, making quantification highly subjective and not reproducible. We deviated from the use of a force platform to quantify the resting time of a mouse in its home cage. The cage containing a mouse was placed on a connected scale for periods of several days. When the mouse was asleep, the signal was that of the device's background noise, corresponding to the so-called resting period. If the signal was different, the period was considered active, regardless of signal intensity. The result is a chronological timeline showing the distribution of activity and rest periods throughout the night and day. Figure 9A shows the timelines for each mouse, grouped by genotype: *Chrna7*^{-/-} (as a control), *ColQ*^{-/-} and double mutant *Chrna7*^{-/-};*ColQ*^{-/-}.

To compare the mice, we calculated several parameters, including the total duration of activity, the mean duration of activity, the number of active periods, and the mean mobility during the night and day (see Methods) (Fig. 9B). During the night, the total duration of mouse activity is similar for mice of different genotypes, but the number and average duration of activity periods for *ColQ*^{-/-} mice are higher and shorter, respectively, than for other genotypes. The mobility of *ColQ*^{-/-} mice is lower than that of *Chrna7*^{-/-};*ColQ*^{-/-} mice, which is lower than that of *Chrna7*^{-/-} mice. Altogether, these results suggest that the $\alpha 7$ /GABA_B receptor-mediated pathway contributes to the fatigability of *ColQ*^{-/-} mice and thus could be a potential pharmacological target.

Discussion

Using complementary approaches, we established a novel regulatory loop in which ACh controls its own release at

the NMJ: when nerve-released ACh reaches $\alpha 7$ nAChR on the TSC, $\alpha 7$ nAChR activation causes GABA secretion via GAT-1. GABA released from the TSC then activates presynaptic GABA_B receptors, which downregulates ACh release.

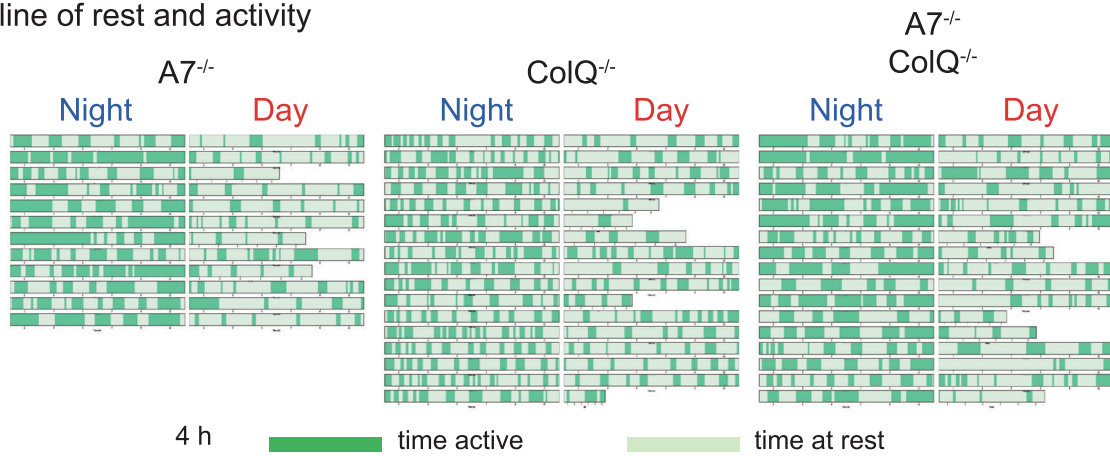
GABA is a gliotransmitter at the mammalian NMJ that can be released independently of Ca²⁺ waves

Our data show that GABA can act as a gliotransmitter at the mouse NMJ. Previous studies have demonstrated that GABA can inhibit the release of ACh at the NMJ in mammals. The exogenous application of GABA at a concentration of 10 μ M was found to decrease quantal content of EPP by 34% at the NMJs of rat diaphragm. The effect of GABA was found to be attenuated following the application of either the GABA_B receptor blocker (CGP

55845) or by an inhibitor of phospholipase C (U73122) (Malomouzh et al., 2015). GABA, GAT-2 and GAD67 were localized by immunofluorescence at the rat NMJs (Nurullin et al., 2018). Given that GAD synthesizes GABA from glutamate, it is pertinent to note that glutamate acts also at the mammalian NMJ (Colombo & Francolini, 2019). To the best of our knowledge, we present for the first time the conditions under which endogenous GABA is released at the NMJ. Our morphological analysis and gene expression also support the production and release of GABA at the NMJ.

TSCs modulate synaptic transmission by releasing gliotransmitters during intracellular TSC Ca²⁺ waves. Indeed, long and high-frequency nerve stimulation can trigger Ca²⁺ waves in the TSC by activating G-coupled receptors (Heredia et al., 2016; Ko & Robitaille, 2015) or by the activation of $\alpha 7$ nAChRs (Noronha-Matos et al., 2020;

A Timeline of rest and activity



B Quantifications

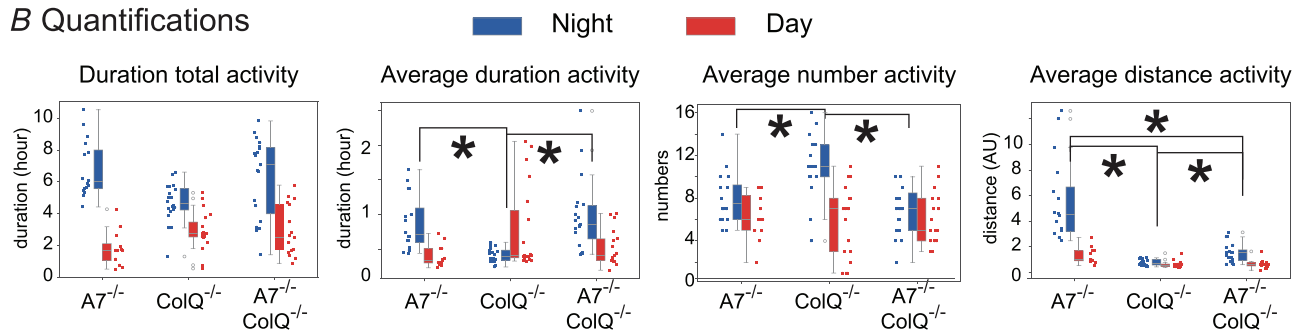


Figure 9. The $\alpha 7$ /GABA_B receptor-mediated pathway contributes to fatigue in the ColQ^{-/-} mouse model
 This experiment was designed to assess fatigability in severely debilitated mice. A sign of fatigability can be the duration of each activity period, thus the more fatigable the shorter the activity period. A second parameter is the distance travelled during the day and night. By placing the cage with a mouse on an electronic scale, we quantified the duration of rest, the duration of activity and the distance travelled by a mouse in its home cage (see Methods). *A*, timeline of rest and activity. The timelines show the time course for periods of rest (light green) and activity (dark green) for consecutive night and day periods for Chrna7^{-/-} mice (*n* = 6), ColQ^{-/-} mice (*n* = 8) and Chrna7^{-/-};ColQ^{-/-} mice (*n* = 8). *B*, quantification of mouse rest. The plots present the duration of total activity, the mean of activity duration (in hours), the mean of distance activity and the mean of number activity during the night (blue) or the day (red) for Chrna7^{-/-} mice (*n* = 6), ColQ^{-/-} mice (*n* = 8) and Chrna7^{-/-};ColQ^{-/-} mice (*n* = 8). [Colour figure can be viewed at wileyonlinelibrary.com]

Petrov et al., 2014). In these experimental conditions, the activation of metabotropic A1 receptors results in a reduction in the release of ACh. However, the depression of ACh release triggered by activation of $\alpha 7$ nAChRs and GABA_B receptors can be observed both in the absence and the presence of Ca²⁺ waves. Without Ca²⁺ waves, GABA release is assumed to result from the inversion of the GAT. However, it is possible that additional mechanism of GABA release is involved in the presence of Ca²⁺ waves in TSCs. For example, it has been shown that GABA can be released via Bestrophin1, a Ca²⁺ activated anion channel (Kilb & Kirischuk, 2022).

The $\alpha 7$ /GABA_B receptor-mediated pathway is activated when ACh reaches the $\alpha 7$ nAChR on the TSC

We found that activation of $\alpha 7$ nAChRs by ACh on TSC is limited by AChE clustered by ColQ in the basal lamina, which reduces the spillover, and by BChE anchored at the membrane of the TSC, which hydrolyses ACh before ACh can reach $\alpha 7$ nAChRs. In mature functional NMJ, the $\alpha 7$ /GABA_B receptor-mediated pathway does not contribute to the regular control of the synaptic transmission, and thus a decrease of EPP amplitude is observed only when the system is challenged by very long stimulation trains.

The $\alpha 7$ /GABA_B receptor-mediated pathway is functional during the post-natal development

Our results show that the $\alpha 7$ /GABA_B receptor-mediated pathway is functional early in postnatal development. Before birth, each endplate makes synaptic contacts with several motor axons. However, after birth, the process of synaptic remodeling is initiated and, by the end of the second postnatal week in rodents, each endplate contacts only one motor nerve ending (Brown et al., 1976; Thompson, 1985). It is therefore conceivable that ACh spillover is quite high during development, partly because AChE activity at the NMJ is low in the early postnatal period, as shown in our and previous studies, and partly because a portion of the nerves are not closely connected to the muscles where AChE begins to accumulate. High ACh spillover may activate the $\alpha 7$ nAChR on TSC, trigger the $\alpha 7$ /GABA_B receptor-mediated pathway and consequently change the amplitude of the EPP by reducing the probability of release. Indeed, we found that the amplitude of the EPP is higher and more stable after blocking GABA_B receptors. On the other hand, the depression of ACh release by the $\alpha 7$ /GABA_B receptor-mediated pathway may be important in controlling the recruitment of a readily releasable pool of synaptic vesicles at the NMJs during the period of polyneuronal innervation. During this period,

ACh is released from three or four nerve endings that may be redundant to trigger the muscle action potential. Therefore, maintaining a pool of synaptic vesicles ready to be released can reduce muscle fatigue.

The $\alpha 7$ /GABA_B receptor-mediated pathway accentuates the fatigability of CMS model mice

When AChE at the NMJ is significantly reduced, ACh spillover may exceed the capacity of BChE to hydrolyse AChE before ACh reaches $\alpha 7$ nAChR and activate the $\alpha 7$ /GABA_B receptor-mediated pathway. A deficit of AChE at the NMJ is a hallmark of human CMS as a result of mutations in the ColQ gene, a collagen that organizes AChE tetramers and clusters them in the basal lamina (Donger et al., 1998; Feng et al., 1999; Mihaylova et al., 2008; Ohno et al., 1998; Wargon et al., 2012). A deficit of AChE at the NMJ results in an excess of ACh, which may act at a different level to affect muscle strength and fatigability. First, AChE deficit alters the shape of the EPP (amplitude and duration) because of the ability of ACh to bind repetitively to muscle nAChRs in the synaptic cleft and thus affect muscle contraction and fatigability (Sigoillot et al., 2016). Second, the density of muscle nAChR is decreased by the direct action of ACh and/or by the interaction of ColQ with LRP4 and the signalling by MuSK (Legay, 2018; Uyen Dao et al., 2023). This reduction could be improved by $\beta 2$ adrenergic receptor agonists (Lee, 2020). The precise mechanism of action remains unclear, and the beneficial effects are observed only after weeks of treatment. Indeed, salbutamol has been demonstrated to alter the morphology of the NMJ in ColQ KO mice, increasing the density of postsynaptic receptors and subsequently enhancing muscle strength of these mice (McMacken et al., 2019). Third, this report demonstrates that AChE deficiency in ColQ-deficient muscle leads to ACh spillover that activates the $\alpha 7$ /GABA_B receptor-mediated pathway to modify ACh release. During a short burst of high frequency nerve stimulation, application of the GABA_B receptor antagonist CGP 55845 (2 μ M) can alter the amplitude of EPPs depending on the frequency of stimulation. Moreover, the critical role of this regulatory loop is revealed by the nocturnal activity of the mouse in the cage, with a shorter duration of active period during the night revealing a fatigability that is reversed in ColQ mice by the genetic elimination of $\alpha 7$ nAChR. To improve the release of ACh, 3,4-diaminopyridine has already been used to treat patients with AChE deficiency, consistent with a contribution of ACh release depression to weakness in patients with end-plate AChE deficiency (Wargon et al., 2012).

In addition to the genetic deficit of AChE at the NMJ, inhibition of ChE is still used to improve NMJ function

in CMS and autoimmune myasthenic syndromes. The positive effect by increasing muscle nAChR activation could be counteracted by the negative depression of ACh from the $\alpha 7$ /GABA_B receptor-mediated pathway not only because the depression may reverse the positive increase of ACh, but also because the fluctuation of EPP properties may affect motor control. If ACh spillover caused by pharmacological, genetic or pathological reduction of AChE in the NMJ depresses ACh release through GABA receptor activation, it may be proposed to use GABA_B receptor antagonists as potential new drug candidates for the symptomatic treatment of myasthenic syndromes, particularly as a replacement or complement to 3,4-diaminopyridine.

References

- Anderson, M. J., & Cohen, M. W. (1974). Fluorescent staining of acetylcholine receptors in vertebrate skeletal muscle. *The Journal of Physiology*, **237**, 385–400.
- Araque, A., Carmignoto, G., Haydon, P. G., Oliet, S. H. R., Robitaille, R., & Volterra, A. (2014). Gliotransmitters travel in time and space. *Neuron*, **81**(4), 728–739.
- Bernard, V., Girard, E., Hrabovska, A., Camp, S., Taylor, P., Plaud, B., & Krejci, E. (2011). Distinct localization of collagen Q and PRiMA forms of acetylcholinesterase at the neuromuscular junction. *Molecular and Cellular Neuroscience*, **46**(1), 272–281.
- Blotnick-Rubin, E., & Anglister, L. (2018). Fine localization of acetylcholinesterase in the synaptic cleft of the vertebrate neuromuscular junction. *Frontiers in Molecular Neuroscience*, **11**, 123.
- Brown, M. C., Jansen, J. K., & van Essen, D. (1976). Polynuclear innervation of skeletal muscle in new-born rats and its elimination during maturation. *The Journal of Physiology*, **261**(2), 387–422.
- del Castillo, J., & Katz, B. (1954). Quantal components of the end-plate potential. *The Journal of Physiology*, **124**(3), 560–573.
- Colombo, M. N., & Francolini, M. (2019). Glutamate at the vertebrate neuromuscular junction: From modulation to neurotransmission. *Cells*, **8**(9), 996.
- Crispino, G., di Pasquale, G., Scimemi, P., Rodriguez, L., Galindo Ramirez, F., De Sisti, R. D., Santarelli, R. M., Arslan, E., Bortolozzi, M., Chiorini, J. A., & Mammano, F. (2011). BAAV mediated GJB2 gene transfer restores gap junction coupling in cochlear organotypic cultures from deaf Cx26Sox10Cre mice. *PLoS ONE*, **6**(8), e23279.
- Cristofari, P., Desplanque, M., Poirel, O., Hébert, A., Dumas, S., Herzog, E., Danglot, L., Geny, D., Gilles, J.-F., Geeverding, A., Bolte, S., Canette, A., Trichet, M., Fabre, V., Daumas, S., Pietrancosta, N., El Mestikawy, S., & Bernard, V. (2022). Nanoscopic distribution of VAcHT and VGLUT3 in striatal cholinergic varicosities suggests colocalization and segregation of the two transporters in synaptic vesicles. *Frontiers in Molecular Neuroscience*, **15**, 991732. Available at: <https://www.frontiersin.org/articles/10.3389/fnmol.2022.991732> [Accessed September 12, 2023].
- Donger, C., Krejci, E., Pou Serradell, A., Eymard, B., Bon, S., Nicole, S., Chateau, D., Gary, F., Fardeau, M., Massoulié, J., & Guicheney, P. (1998). Mutation in the human acetylcholinesterase-associated collagen gene, COLQ, is responsible for congenital myasthenic syndrome with end-plate acetylcholinesterase deficiency (Type Ic). *American Journal of Human Genetics*, **63**(4), 967–975.
- Farshadyeganeh, P., Nazim, M., Zhang, R., Ohkawara, B., Nakajima, K., Rahman, M. A., Nasrin, F., Ito, M., Takeda, J., Ohe, K., Miyasaka, Y., Ohno, T., Masuda, A., & Ohno, K. (2023). Splicing regulation of GFPT1 muscle-specific isoform and its roles in glucose metabolisms and neuromuscular junction. *IScience*, **26**(10), 107746.
- Feng, G., Krejci, E., Molgo, J., Cunningham, J. M., Massoulié, J., & Sanes, J. R. (1999). Genetic analysis of collagen Q: Roles in acetylcholinesterase and butyrylcholinesterase assembly and in synaptic structure and function. *Journal of Cell Biology*, **144**(6), 1349–1360.
- Fowler, S. C., Birkestrand, B. R., Chen, R., Moss, S. J., Vorontsova, E., Wang, G., & Zarccone, T. J. (2001). A force-plate actometer for quantitating rodent behaviours: Illustrative data on locomotion, rotation, spatial patterning, stereotypies, and tremor. *Journal of Neuroscience Methods*, **107**(1–2), 107–124.
- Fuertes-Alvarez, S., & Izeta, A. (2021). Terminal Schwann cell aging: Implications for age-associated neuromuscular dysfunction. *Aging and Disease*, **12**(2), 494–514.
- Grundy, D. (2015). Principles and standards for reporting animal experiments in The journal of physiology and experimental physiology. *Experimental Physiology*, **100**(7), 755–758.
- Hartzell, H. C., Kuffler, S. W., & Yoshikami, D. (1975). Post-synaptic potentiation: Interaction between quanta of acetylcholine at the skeletal neuromuscular synapse. *The Journal of Physiology*, **251**(2), 427–463.
- Hastings, R. L., Avila, M. F., Suneby, E., Juros, D., O'young, A., Peres da Silva, J., & Valdez, G. (2023). Cellular and molecular evidence that synaptic Schwann cells contribute to aging of mouse neuromuscular junctions. *Aging Cell*, **22**(11), e13981.
- Heredia, D. J., Schubert, D., Maligireddy, S., Hennig, G. W., & Gould, T. W. (2016). A novel striated muscle-specific myosin-blocking drug for the study of neuromuscular physiology. *Frontiers in Cellular Neuroscience*, **10**, 276.
- Hernandez, C. M., Cortez, I., Gu, Z., Colón-Sáez, J. O., Lamb, P. W., Wakamiya, M., Yakel, J. L., & Dineley, K. T. (2014). Research tool: validation of floxed $\alpha 7$ nicotinic acetylcholine receptor conditional knockout mice using in vitro and in vivo approaches. *The Journal of Physiology*, **592**(15), 3201–3214.
- Kilb, W., & Kirischuk, S. (2022). GABA RELEASE from astrocytes in health and disease. *International Journal of Molecular Sciences*, **23**(24), 15859.
- Ko, C.-P., & Robitaille, R. (2015). Perisynaptic Schwann cells at the neuromuscular synapse: Adaptable, multitasking glial cells. *Cold Spring Harbor Perspectives in Biology*, **7**(10), a020503.

- Lee, Y. I. (2020). Developmental neuromuscular synapse elimination: Activity-dependence and potential downstream effector mechanisms. *Neuroscience Letters*, **718**, 134724.
- Legay, C. (2018). Congenital myasthenic syndromes with acetylcholinesterase deficiency, the pathophysiological mechanisms. *Annals of the New York Academy of Sciences*, **1413**(1), 104–110.
- Lenina, O. A., Zueva, I. V., Zobov, V. V., Semenov, V. E., Masson, P., & Petrov, K. A. (2020). Slow-binding reversible inhibitor of acetylcholinesterase with long-lasting action for prophylaxis of organophosphate poisoning. *Scientific Reports*, **10**(1), 16611.
- Lomo, T. (2003). What controls the position, number, size, and distribution of neuromuscular junctions on rat muscle fibers? *Journal of Neurocytology*, **32**(5–8), 835–848.
- Madisen, L., Mao, T., Koch, H., Zhuo, J.-M., Berenyi, A., Fujisawa, S., Hsu, Y.-W. A., Garcia, A. J., Gu, X., Zanella, S., Kidney, J., Gu, H., Mao, Y., Hooks, B. M., Boyden, E. S., Buzsáki, G., Ramirez, J. M., Jones, A. R., Svoboda, K., Han, X., Turner, E. E., & Zeng, H. (2012). A toolbox of Cre-dependent optogenetic transgenic mice for light-induced activation and silencing. *Nature Neuroscience*, **15**(5), 793–802.
- Madisen, L., Zwingman, T. A., Sunkin, S. M., Oh, S. W., Zariwala, H. A., Gu, H., Ng, L. L., Palmiter, R. D., Hawrylycz, M. J., Jones, A. R., Lein, E. S., & Zeng, H. (2010). A robust and high-throughput Cre reporting and characterization system for the whole mouse brain. *Nature Neuroscience*, **13**(1), 133–140.
- Magnaghi, V., Ballabio, M., Camozzi, F., Colleoni, M., Consoli, A., Gassmann, M., Lauria, G., Motta, M., Procacci, P., Trovato, A. E., & Bettler, B. (2008). Altered peripheral myelination in mice lacking GABAB receptors. *Molecular and Cellular Neuroscience*, **37**(3), 599–609.
- Malomouzh, A. I., Petrov, K. A., Nurullin, L. F., & Nikolsky, E. E. (2015). Metabotropic GABAB receptors mediate GABA inhibition of acetylcholine release in the rat neuromuscular junction. *Journal of Neurochemistry*, **135**(6), 1149–1160.
- Matsuoka, T., Ahlberg, P. E., Kessar, N., Iannarelli, P., Dennehy, U., Richardson, W. D., McMahon, A. P., & Koentges, G. (2005). Neural crest origins of the neck and shoulder. *Nature*, **436**(7049), 347–355.
- McMacken, G. M., Spendiff, S., Whittaker, R. G., O'Connor, E., Howarth, R. M., Boczonadi, V., Horvath, R., Slater, C. R., & Lochmüller, H. (2019). Salbutamol modifies the neuromuscular junction in a mouse model of ColQ myasthenic syndrome. *Human Molecular Genetics*, **28**(14), 2339–2351.
- Mihaylova, V., Müller, J. S., Vilchez, J. J., Salih, M. A., Kabiraj, M. M., D'Amico, A., Bertini, E., Wölfle, J., Schreiner, F., Kurlemann, G., Rasic, V. M., Siskova, D., Colomer, J., Herczegfalvi, A., Fabriciova, K., Weschke, B., Scola, R., Hoellen, F., Schara, U., Abicht, A., & Lochmüller, H. (2008). Clinical and molecular genetic findings in COLQ-mutant congenital myasthenic syndromes. *Brain*, **131**(3), 747–759.
- Minic, J., Chatonnet, A., Krejci, E., & Molgó, J. (2003). Butyrylcholinesterase and acetylcholinesterase activity and quantal transmitter release at normal and acetylcholinesterase knockout mouse neuromuscular junctions. *British Journal of Pharmacology*, **138**(1), 177–187.
- Minic, J., Molgó, J., Karlsson, E., & Krejci, E. (2002). Regulation of acetylcholine release by muscarinic receptors at the mouse neuromuscular junction depends on the activity of acetylcholinesterase. *European Journal of Neuroscience*, **15**(3), 439–448.
- Noronha-Matos, J. B., Oliveira, L., Peixoto, A. R., Almeida, L., Castellão-Santana, L. M., Ambiel, C. R., Alves-do Prado, W., & Correia-de-Sá, P. (2020). Nicotinic $\alpha 7$ receptor-induced adenosine release from perisynaptic Schwann cells controls acetylcholine spillover from motor endplates. *Journal of Neurochemistry*, **154**(3), 263.
- Nurullin, L. F., Nikolsky, E. E., & Malomouzh, A. I. (2018). Elements of molecular machinery of GABAergic signaling in the vertebrate cholinergic neuromuscular junction. *Acta Histochemica*, **120**(3), 298–301.
- Ohno, K., Brengman, J., Tsujino, A., & Engel, A. G. (1998). Human endplate acetylcholinesterase deficiency caused by mutations in the collagen-like tail subunit (ColQ) of the asymmetric enzyme. *Proceedings National Academy of Science USA*, **95**(16), 9654–9659.
- Ohno, K., Engel, A. G., Brengman, J. M., Shen, X.-M., Heidenreich, F., Vincent, A., Milone, M., Tan, E., Demirci, M., Walsh, P., Nakano, S., & Akiyuchi, I. (2000). The spectrum of mutations causing end-plate acetylcholinesterase deficiency. *Annals of Neurology*, **47**(2), 162–170.
- Palacín, M., Estévez, R., Bertran, J., & Zorzano, A. (1998). Molecular biology of mammalian plasma membrane amino acid transporters. *Physiological Reviews*, **78**(4), 969–1054.
- Petrov, K. A., Girard, E., Nikitashina, A. D., Colasante, C., Bernard, V., Nurullin, L., Leroy, J., Samigullin, D., Colak, O., Nikolsky, E., Plaud, B., & Krejci, E. (2014). Schwann cells sense and control acetylcholine spillover at the neuromuscular junction by $\alpha 7$ nicotinic receptors and butyrylcholinesterase. *Journal of Neuroscience*, **34**(36), 11870–11883.
- Prieto, C., & Barrios, D. (2020). RaNA-Seq: Interactive RNA-Seq analysis from FASTQ files to functional analysis ed. Berger B. *Bioinformatics*, **36**(6), 1955–1956.
- Rochon, D., Rouse, I., & Robitaille, R. (2001). Synapse-Glia Interactions at the Mammalian Neuromuscular Junction. *Journal of Neuroscience*, **21**(11), 3819–3829.
- Sanes, J. R., & Lichtman, J. W. (1999). Development of the vertebrate neuromuscular junction. *Annual Review of Neuroscience*, **22**(1), 389–442.
- Sigoillot, S. M., Bourgeois, F., Karmouch, J., Molgó, J., Dobbertin, A., Chevalier, C., Houlgatte, R., Léger, J., & Legay, C. (2016). Neuromuscular junction immaturity and muscle atrophy are hallmarks of the ColQ-deficient mouse, a model of congenital myasthenic syndrome with acetylcholinesterase deficiency. *The Federation of American Societies for Experimental Biology Journal*, **30**(6), 2382–2399.

- Skok, M. V., Voitenko, L. P., Voitenko, S. V., Y Lykhmus, E., Kalashnik, E. N., Litvin, T. I., Tzartos, S. J., & Skok, V. I. (1999). Alpha subunit composition of nicotinic acetylcholine receptors in the rat autonomic ganglia neurons as determined with subunit-specific anti- α (181–192) peptide antibodies. *Neuroscience*, **93**(4), 1427–1436.
- Slater, C. R. (2017). The structure of human neuromuscular junctions: Some unanswered molecular questions. *International Journal of Molecular Sciences*, **18**(10), 2183.
- Takada, Y., Beyer, L. A., Swiderski, D. L., O'neal, A. L., Prieskorn, D. M., Shivatzki, S., Avraham, K. B., & Raphael, Y. (2014). Connexin 26 null mice exhibit spiral ganglion degeneration that can be blocked by BDNF gene therapy. *Hearing Research*, **309**, 124–135.
- Thompson, W. J. (1985). Activity and synapse elimination at the neuromuscular junction. *Cellular and Molecular Neurobiology*, **5**(1–2), 167–182.
- Todd, K. J., Darabid, H., & Robitaille, R. (2010). Perisynaptic glia discriminate patterns of motor nerve activity and influence plasticity at the neuromuscular junction. *Journal of Neuroscience*, **30**(35), 11870–11882.
- Truong, C., Oudre, L., & Vayatis, N. (2020). Selective review of offline change point detection methods. *Signal Processing*, **167**, 107299.
- Uyen Dao, T. M., Barbeau, S., Messéant, J., Della-Gaspera, B., Bouceba, T., Semprez, F., Legay, C., & Dobbertin, A. (2023). The collagen ColQ binds to LRP4 and regulates the activation of the Muscle-Specific Kinase/LRP4 receptor complex by agrin at the neuromuscular junction. *Journal of Biological Chemistry*, **299**(8), 104962.
- Wargon, I., Richard, P., Kuntzer, T., Sternberg, D., Nafissi, S., Gaudon, K., Lebaill, A., Bauche, S., Hantai, D., Fournier, E., Eymard, B., & Stojkovic, T. (2012). Long-term follow-up of patients with congenital myasthenic syndrome caused by COLQ mutations. *Neuromuscular Disorders*, **22**(4), 318–324.

Additional information

Data availability statement

All data underlying the results are available as part of the article and no additional source data is required. The code describing Quantification of mouse activity in home cage is available at <https://github.com/deepcharles/mousemonitor>.

Competing interests

The authors declare that they have no competing interests.

Author contributions

K.P. and E.K. were responsible for the study hypothesis and design. Material preparation, data collection and analysis were performed by O.L., K.P., L.N., G.S. and D.S. in Kazan; by T.G. and C.T. at Université Paris Cité Saclay, V.B. at Sorbonne Université, and E.K. and K.P. at Université Paris Cité in Paris; and by K.O. at Nagoya University of Arts and Sciences in Nagoya. K.P. and E.K. wrote the first draft of the manuscript. All authors commented on previous versions of the manuscript. All authors read and approved the final version of the manuscript submitted for publication.

Funding

This work was supported by AFM-telethon (grants 21008 and 23138) to E.K.; by the Russian Science Foundation (grant no. 24-15-00249) to O.L. and K.P. for part of electrophysiological experiments on newborn mice. We gratefully acknowledge CSF-SAC FRC KSC RAS for providing the necessary facilities to carry out the immunofluorescence experiments. L.N., G.S. and D.S. were supported by an assignment for FRC Kazan Scientific Center of RAS.

Acknowledgements

We acknowledge Axelle Desoignies and Isis Blanchard from Mouse facility (Plateforme hébergement et d'élevage/UAR2009/US36) for management of mice, as well as Lyle Graham for critical editing.

Keywords

acetylcholine, acetylcholinesterase, aminobutyric acid, neuromuscular junction

Supporting information

Additional supporting information can be found online in the Supporting Information section at the end of the HTML view of the article. Supporting information files available:

Peer Review History